AD-A269 684

(4)

Technical Report 1571
January 1993

Evaporation Duct Communication:

Measurement Results

L. T. Rogers
K. D. Anderson

DTIC
S ELECTE
SEP 22 1993
E D

NRaD

93-21971

Technical Report 1571
January 1993

Evaporation Duct Communication:

Measurement Results

L. T. Rogers
K. D. Anderson

Accesion For		
NTIS CRA&I		☒
DTIC TAB		☐
Unannounced		☐
Justification		
By		
Distribution /		
Availability Codes		
Dist	Avail and / or Special	
A-1		

**NAVAL COMMAND, CONTROL AND
OCEAN SURVEILLANCE CENTER
RDT&E DIVISION
San Diego, California 92152–5001**

J. D. FONTANA, CAPT, USN
Commanding Officer

R. T. SHEARER
Executive Director

ADMINISTRATIVE INFORMATION

Released by
R. A. Paulus, Head
Tropospheric Branch

Under authority of
J. H. Richter, Head
Ocean and Atmospheric
Sciences Division

RV

EXECUTIVE SUMMARY

OBJECTIVES

The Evaporation Duct Communication (EDCOM) project evaluates an alternative ship-to-ship communication channel that exploits the natural environment. It is a unique project using a microwave communication circuit (similar to the commercial line-of-sight [LOS] microwave links that carry voice and data across the country) on an over-water, over-the-horizon (OTH) path where successful communication depends on the evaporation duct. A one-way 83-km transmission path is instrumented to simultaneously measure surface meteorological conditions and radio frequency (RF) characteristics of the communication channel. Received Signal Levels (RSL) measurements are compared to propagation model RSL predictions that are based on knowledge of the surface meteorology. Percent Error-Free Seconds (%EFS), Bit-Error Rate (BER) and other industry standard parameters of digital link performance are measured at DS−1 transmission rates (1.544 megabits per second). These measurements are used to validate and to improve the propagation models so that the performance of similar communication circuits can be predicted from knowledge of the environmental conditions.

RESULTS

The principal results of the EDCOM project are as follows:

1. First, EDCOM has provided experimental data to assess the validity of a propagation model used for the development and design of an alternative Super High Frequency (SHF) link for U.S. Navy ship-to-ship communications.

2. EDCOM has demonstrated the reliability of an OTH communication link that depends on the evaporation duct for successful link operation.

3. EDCOM has provided statistics required for optimal code design for the digital link.

RECOMMENDATIONS

1. The low percentage of successful communications (about 25%) strongly suggests that the development and design of a SHF link focus on a system that does not rely on the evaportion duct for enhanced communication capabilities. It is recommended that the SHF link be designed for LOS ranges where availabilities of 99.99% or better can be achieved.

2. It is recommended that the frequency selection for a LOS system consider evaporation ducting effects. Communication to ranges of twice LOS for lower frequency (1 to 5 GHz) systems will occur infrequently; whereas, for higher frequency (5 to 14 GHz) systems, twice LOS ranges are observed about 25% of the time.

3. It is recommended that further studies be made to optimize signal coding and protocol procedures during bursty channel conditions.

CONTENTS

FIGURES

TABLES

INTRODUCTION

This report provides results from an experiment testing the feasibility of using the evaporation duct to support an alternative high-speed communication system for Navy applications. The feasibility of this link was discussed in an earlier study (Anderson, 1991), and preparation for the experiment, including software development and transmitter and receiver site preparation, was documented in a progress report (Anderson and Rogers, 1991). In this report, meteorological and RF propagation models are reviewed. Data from the EDCOM propagation experiment are summarized and are used to assess RF propagation model predictions that are derived from climatology. EDCOM digital link performance statistics are presented and are related to actual and predicted average RSL values. Additionally, high-speed, time-series analysis is provided for code word and network protocol design.

EDCOM simulates a realistic ship-to-ship communication link. Antenna heights are typical of shipboard installations, as they are approximately 25 m above the ocean surface. This height corresponds to a 41.2-km line-of-sight (LOS) distance between transmit and receive sites. The EDCOM path, between the transmitter at San Mateo Point and the receiver in Point Loma, is 83.1 km in length, which is more than twice the LOS range. A map of the southern California coastline from Point Loma (San Diego) to San Mateo Point (the northern coastal point of Camp Pendleton) is shown in figure 1. The figure shows both transmitter and receiver sites and their line-of-sight horizon.
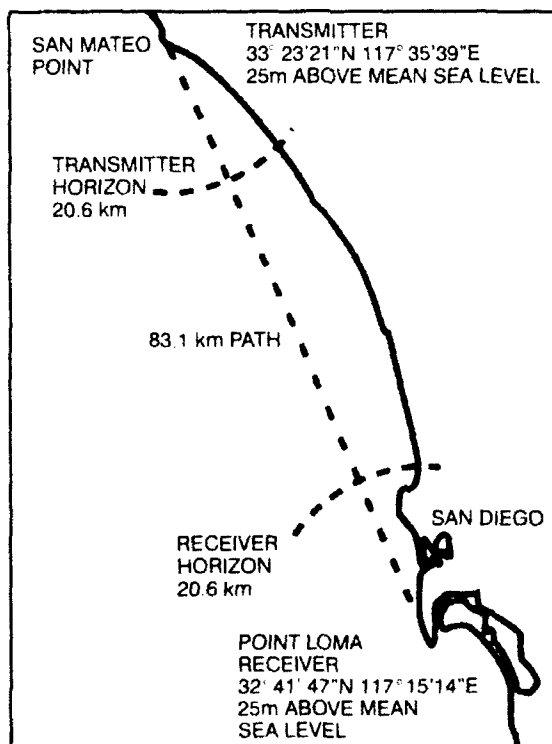
Figure 1. Southern California coastline showing EDCOM transmission path and transmitter and receiver horizons.

Two frequencies (7.5 and 14.5 GHz) are used to assess propagation effects. Commercial digital radio equipment (Loral/Terracom models TCM-624B and TCM-628B) is used in a simplex mode (one-way transmission) to reduce costs. Industry-standard DS-1 digital transmission test sets (DTTS), Tautron model 5108s, are used to generate a quasi-random bit stream at a rate of 1.544 Mb/s (DS-1), and are used to analyze the received bit stream in terms of bit-error rate (BER) and block-error rate (fixed-time-interval blocks that contain errors). Figure 2 is the transmit site equipment with the transmitter units situated below the associated DTTS. The receive site equipment is similar in appearance.
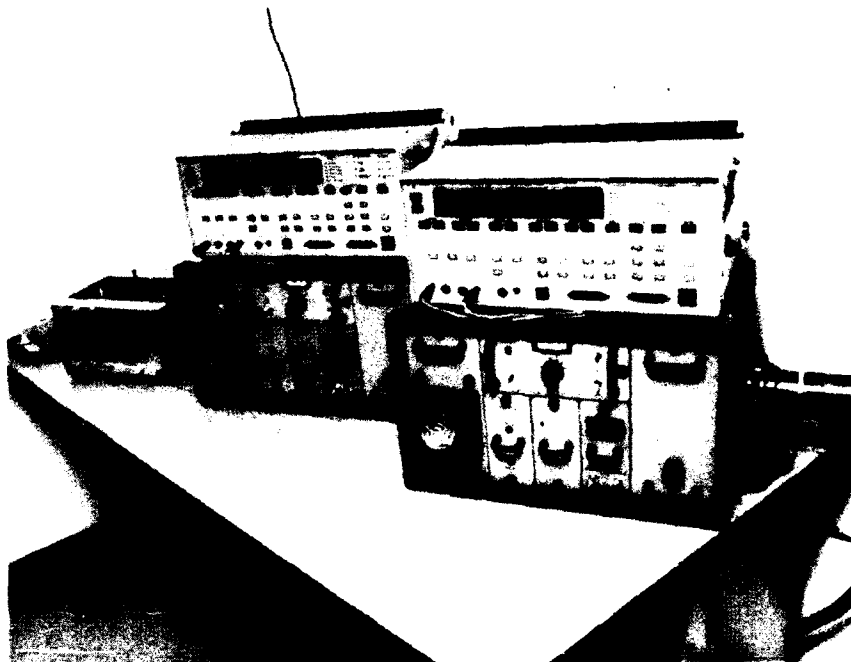
Figure 2. Transmit site equipment showing digital transmission
test sets (top) and transmitters (bottom).

The transmit site at San Mateo Point is shown in figure 3. At the top of the mast is the anemometer and wind vane assembly. The upper parabolic dish is the 14.5-GHz transmit antenna and the box behind it is the transmitter RF module. Immediately below the dish is the 7.5-GHz transmit antenna and its associated transmitter RF module. On the ground and to the left, is the instrument hut containing the Rotronics temperature and humidity probe. To the right is the van that houses the remainder of the transmit site equipment. Although it is not easily decernible from the photograph, this patch of land is a bluff approximately 20 m above mean sea level (MSL).
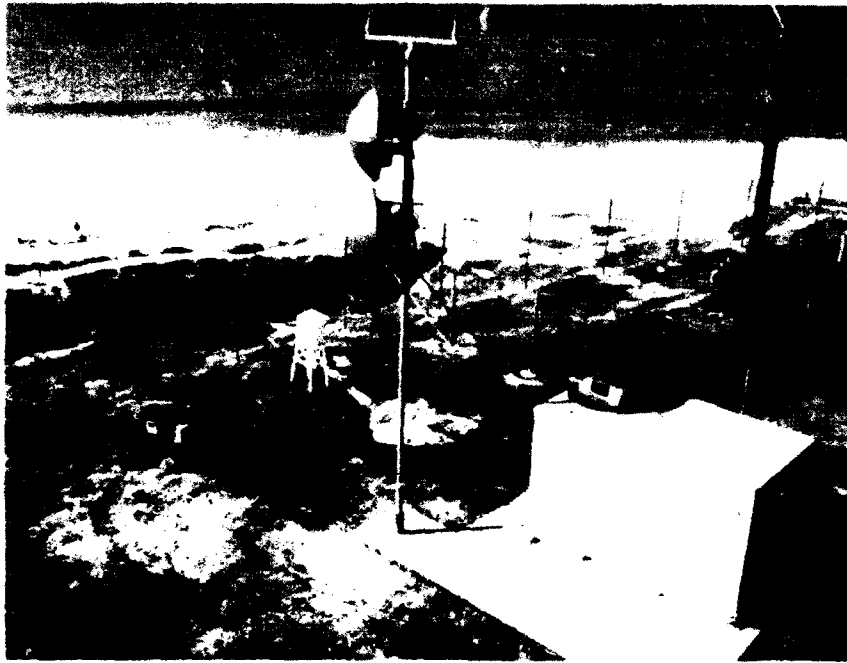
Figure 3. Transmit site at San Mateo Point, California.

Figure 4 is a photograph of the receive site located in Building 599 at the NCCOSC RDT&E facility, San Diego, California. The instrument hut housing the Rotronics temperature and humidity probe is to the right and at the end of the pier. Nearby are the anemometer and wind vane on a post. Two infrared sensors for measurement of sea-surface temperature are mounted on the pier handrail.

Experimental measurements show that actual RSL enhancements (in dB), due to evaporation ducting, are roughly 75% of those predicted by climatological-based propagation models for both 7.5 and 14.5 GHz. RSL exceeds the instantaneous received signal level (IRSL) required for error-free communication 27% of the time at 14.5 GHz, and 34% of the time at 7.5 GHz. The channel is a bursty channel. Relatively small amounts of power (less than 5 dB) are required to go from 50% error-free seconds (%EFS) to 90 or 95 %EFS as measured over 5-minute intervals. Substantially more power is required to achieve 99 %EFS.

3
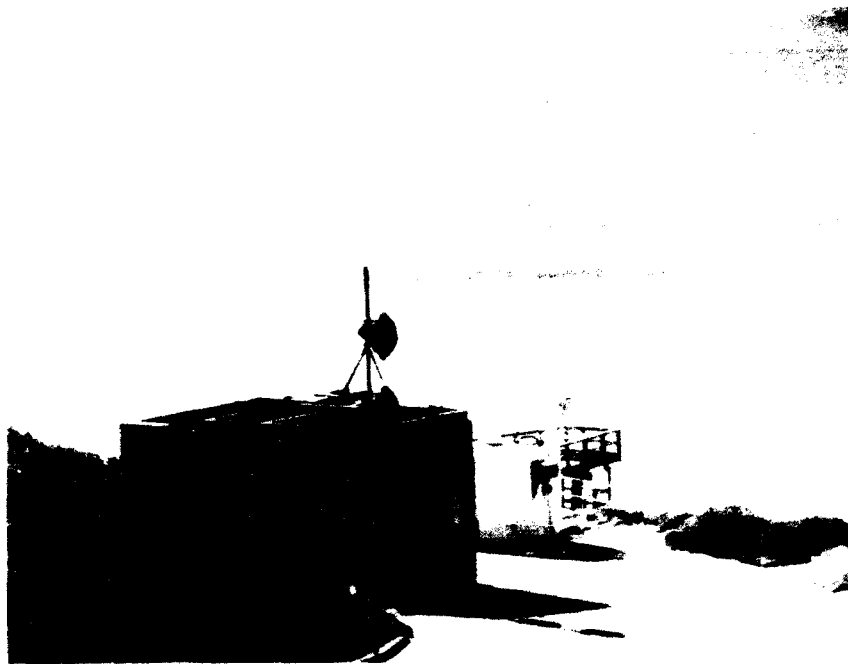
Figure 4. Receive site at building 599, NCCOSC RDT&E facility,
San Diego, California.

METEOROLOGICAL AND PROPAGATION MODELS

The evaporation duct has been recognized for many years as a propagation phenome-
non that can increase beyond-horizon radio signals by many dB's above diffraction field
levels for frequencies above 2 GHz (Hitney, et al., 1985). Turbulent mixing in the surface
layer (air-sea boundary) causes a rapid decrease in the water-vapor content of the air,
which, in turn, creates a strong negative radio refractivity gradient that forms an evapora-
tive duct. This duct acts as a leaky wave guide. An RF signal can propagate with a low
attenuation rate within the guide that is bounded by the sea surface and the evaporation
duct height. At ranges beyond the normal radio horizon, the field strength in the duct may
be 10 to 100 dB greater than the diffraction field strength. Above the duct, the RF field
strength decreases rapidly; however, due to leakage from the duct, the signal strengths may
still be substantially higher than the diffraction field. The signal enhancement depends
strongly on frequency because these ducts are vertically thin, typically less than 20 m.

In practice, boundary-layer theory relates bulk surface meteorological measurements of
air temperature, sea temperature, wind speed, and humidity to the evaporation duct height.
Evaporation duct height is computed using the Jeske (1971) model as implemented by
Hitney (1975) with thermal stability modifications suggested by Paulus (1985). In a ther-
mally neutral atmosphere (where the air-sea temperature difference is zero) the modified
refractivity profile $M(z)$ is

$$M(z) = M(0) + 0.125(z - (\delta + z_0)\ln[(z + z_0)/z_0])$$ (1)

where z is height above the ocean, δ is evaporation duct height, and z_0 is a length characterizing boundary roughness.

Numerical propagation modeling techniques agree with RF measurement results when single-station surface meteorological observations are available to determine the refractivity-versus-altitude profile of the evaporation duct (Katzin, Bauchman and Binnian, 1947; Richter and Hitney, 1988; Anderson, 1990). When the atmospheric refractivity profile above the evaporation duct height is a *standard* profile ($M(z)$ is monotonically decreasing at a rate of 118 M/km), the evaporation duct is the dominant mode of propagation. *Nonstandard* atmospheric refractivity profiles, particularly surface-based ducts, can raise received signal levels beyond LOS ranges several dB's above free-space levels, often 20 dB or more above the already enhanced signal levels that are seen when there is a standard refractivity profile above the evaporation duct height. When the refractivity profile above the evaporation duct height is neither standard nor nearly so, the evaporation duct may not be the dominant propagation mode. In the San Diego area, where the EDCOM experiment took place, nonstandard atmospheric refractivity profiles (which include surface-based and elevated ducts) are common. Table 1 provides percentages of soundings that indicate the presence of surface-based and elevated ducts in the San Diego area (Patterson, 1987). Of the 86 atmospheric soundings taken at Montgomery field in San Diego during the EDCOM experiment, only 53 (62%) show *standard* or nearly *standard* refractivity profiles. To validate the model for predicting the usefulness of the evaporation duct as an alternative communications channel, it is therefore necessary to separate RSL data that are associated with standard atmospheric refractivity profiles above the evaporation duct height from those that are not.

Table 1. Percentage of occurrences for surface-based and elevated ducts in San Diego, CA.

Duct Type	Month/% Occurrence					
	Jan	Feb	Mar	Apr	May	Avg. (%)
Surface-based Ducts						
Day	18	18	20	17	18	18.2
Night	24	24	18	14	11	8.2
Elevated Ducts						
Day	27	27	31	41	48	34.8
Night	39	39	44	55	73	50.0

The waveguide propagation model, known as *MLAYER*, was originally developed by Baumgartner (1983) and was briefly described by Hitney, et al. (1985). *MLAYER*, based on the formalism developed by Budden (1961), solves the modal equation for an arbitrary

vertical, multiple-linear-segment refractivity profile using a root-finding scheme that locates all modes with attenuation rates less than a specified value. Surface roughness is accounted for by modifying the surface-reflection coefficient, which is based on the wind speed. Horizontal homogeneity of refractive conditions is assumed.

Measurements of ambient air temperature, sea temperature, wind speed, and relative humidity are used to calculate the evaporation duct height δ. Equation 1 is used to calculate the vertical refractivity profile $M(z)$ that is needed by the *MLAYER* program. Measured wind speed is used to calculate the surface roughness parameter σ, which is also used by *MLAYER*.

RECEIVE SITE INSTRUMENTATION

All receive site data acquisition is controlled from a standard 386AT personal computer. A National Instruments AT-MIO-16 analog-to-digital (A/D) board is installed to provided eight differential voltage channels for analog input. Two RS-232 ports provide serial communications with DTTS. A block diagram of this configuration is shown in figure 5. All meteorological and RSL measurements are made using the eight analog A/D channels. Table 2 lists analog input channel numbers, the parameters that are actually recorded to disk, and the parameter ranges. Wind direction (Ch. 0) is used for determining if the airflow is onshore (coming from ≈ 160 to 340 degrees true) or continental (≈ 340 to 160 degrees true). Wind speed, air temperature, relative humidity, and sea temperature (Ch 1-4, respectively) are used for computing the surface layer M profile that, in turn, is used for predicting signal levels. The combined 7.5 GHz and 14.5 GHz fault bus (Ch. 5) provides indication of equipment malfunctions or signal levels below detection values. Channels 6 and 7 sense the automatic gain control (AGC) voltage, which is inversely proportional to the received signal level measured in dB. The AGC voltage is used for continuous sampling of the received signal level.

WIND DIRECTIONS (CH 0)
WIND SPEED (CH 1)
AIR TEMPERATURE (CH 2)
RELATIVE HUMIDITY (CH 3)
SEA TEMPERATURE (CH 4)
14.5 GHz FAULT BUS (CH 5)
7.5 GHz FAULT BUS (CH 5)
7.5 GHz AGC (CH 6)
14.5 GHz AGC (CH 7)

14.5 GHz
PARABOLIC
ANTENNA

7.5 GHz
PARABOLIC
ANTENNA

SIGNAL
SCALING
AND
COMBINING
CKTS

LORAL
TCM 624B
RECEIVER
7.5 GHz

LORAL
TCM 628A
RECEIVER
14.5 GHz

TAUTRON
5108

TAUTRON
5108

DIGITAL
TRANSMISSION
TEST SETS

RS – 232 SERIAL PORT

RS – 232 SERIAL PORT

NATIONAL INSTRUMENTS
AT – MIO – 16
ANALOG TO DIGITAL
BOARD

MULTI-
COMM
4 X RS232
BOARD

RECEIVE SITE
386AT PERSONAL COMPUTER

Figure 5. Receive site functional diagram.

Table 2. Analog input channels.

Ch.	Parameter	Parameter Range
0	Wind Direction	0 to 360 deg.
1	Wind Speed	0 to 86.8 knots
2	Air Temperature	-20 to 55°C
3	Relative Humidity	0 to 100 % rh
4	Sea Temperature	0 to 100°C
5	Combined Fault Bus	0 to 4.5 v
6	7.5 GHz AGC voltage	$+1$ to -4 v
7	14.5 GHz AGC voltage	$+1$ to -4 v

7

To comply with a maximum of 8 available analog channels, the 7.5 and 14.5 GHz fault busses are combined by a voltage addition circuit in channel 5. Both channels 6 and 7 use scaling circuits (voltage divider networks) to divide the AGC voltages by a factor of 3 to reduce the signal within the range of the A/D board. All receiver testing and system operation utilizes this configuration. (For the remainder of this paper, the term AGC voltage refers to this divided signal.)

Digital signal quality measurements of the receiver are listed in table 3. The first of these measurements is the average bit-error rate (BER). The next three measurements are block-error rates: error seconds (ES), counting of seconds in a given block of time when at least one bit error has occurred; severely errored seconds (SES), counting of seconds in a given block of time when the bit-error rate exceeds 10^{-3}; and percent error-free seconds (%EFS), computing the percentage of seconds when an error has not occurred. Additionally, DSX amplitude, the amplitude of the T-1 input signal to the DTTS, is measured for indication of receiver problems.

Table 3. Receive digital signal quality measurements.

Measurement	Description
Average BER	Average Bit-Error Rate
ES	Error Seconds
SES	Severely Errored Seconds ($> 10^{-3}$ BER)
%EFS	Percent Error-Free Seconds
DSX Amplitude	Peak Voltage of T-1 Signal

TRANSMIT SITE INSTRUMENTATION

Transmitter analog instrumentation at San Mateo Point is similar to that at the receive site in San Diego, except that channel 4 is unused because there is no sea temperature probe. At the transmitter site, channels 6 and 7 sense the transmit power signal instead of the AGC voltage as is done at the receive site. Measurements of transmit site meteorological parameters are used for assessing path homogeneity. Only two measurements (DSX amplitude and BER) of the digital signal quality are performed hourly to verify the quality of the generated T-1 signal being sent from the DTTS to the transmitters. An additional feature is the use of a third RS-232 serial port and a modem to send, by phoneline, each day's data file to a receive site computer.

INSTRUMENT SCHEDULING

Scheduling for data acquisition is similar for both sites. At the receive site, the control program runs a 5-minute test every 6 minutes, thereby allowing a minute for processing and recording data. At the beginning of the test interval, each bit-error rate tester is commanded to begin an autonomous 5-minute test. At the same time, the computer via the D/A

8

board begins sampling of analog parameters at 5-second intervals. After slightly more than 5 minutes have elapsed, each DTTS is interrogated to obtain received digital signal quality measurements; the sampled analog measurements are subsequently averaged. Both sets of measurements are then recorded to the disk in ASCII text format.

TRANSMITTER AND RECEIVER TESTING

The rated and measured transmitter power and receiver/sensitivity data are compared in table 4. Output power measurement for each transmitter is obtained by using a Hewlett-Packard HP−438A power meter as shown in figure 6. In the test setup, two variable attenuators with necessary connectors and cabling are installed between the transmitter and the receiver. A DTTS is utilized for both signal generation (for data input to the transmitter) and signal quality measurement (for the data output of the receiver). Attenuation is gradually increased and then decreased while the computer records both the BER and the AGC voltage. Figure 7 shows BER and AGC voltage versus RSL and propagation factor (PF) in dB for both the 7.5-GHz and the 14.5-GHz receivers. The propagation factor is a convention whereby the received signal level is referenced to the expected received signal level for free space propagation over the described path geometry and link parameters. From figure 7, the following findings are apparent:

- AGC voltage varies nearly linearly with the propagation factor in the range $-40 \leq PF \leq 0$.

- At both frequencies, the signal is essentially error free (BER $\leq 10^{-6}$) at propagation factors greater than -30 dB; any information in the signal is lost (BER $\geq$ 0.75) when the propagation factor is less than approximately -35 dB.

In figure 7, the receiver sensitivity (the minimum received signal strength below which the error rate is greater than 10^{-6} BER) is obtained from the BER versus propagation factor curve. Both rated and measured values of receiver sensitivity are included in table 4. Slope and intercept formulas (equations 2 and 3) are developed from the linear portion of the AGC voltage versus RSL curves in figure 7.

$$RSL_{7.5GHz} = -88.5dBm - 10.37 \times V_{7.5AGC} \qquad (2)$$

$$RSL_{14.5GHz} = -93dBm - 10.4 \times V_{14.5AGC} \qquad (3)$$

Table 4. Loral Terracom transmitter and receiver rated and measured specifications.

Frequency Loral Model Number	7.5 GHz TCM-624A		14.5 GHz TCM-628B	
	Rated	Measured	Rated	Measured
Transmitter Power (W)	0.66	0.87	0.20	0.21
Transmitter Power (dBm)	28.2	29.4	23.0	23.2
Receiver Sensitivity (dBm) @ 1.0E-6 BER	−88.5	−78.0	−86.5	−78.0
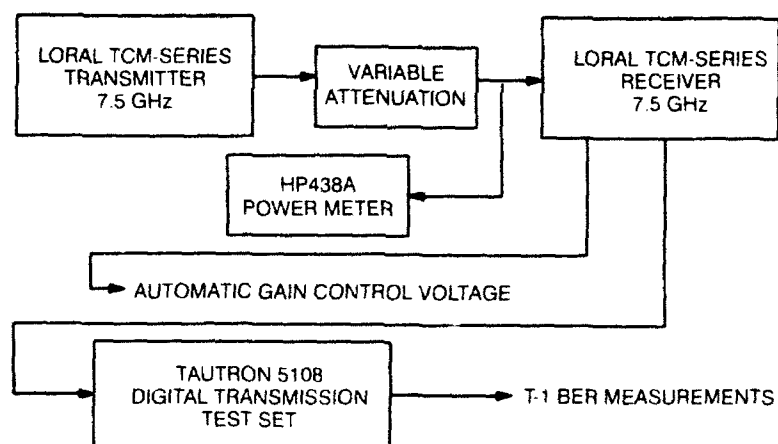
Figure 6. 7.5-GHz system testing arrangement.
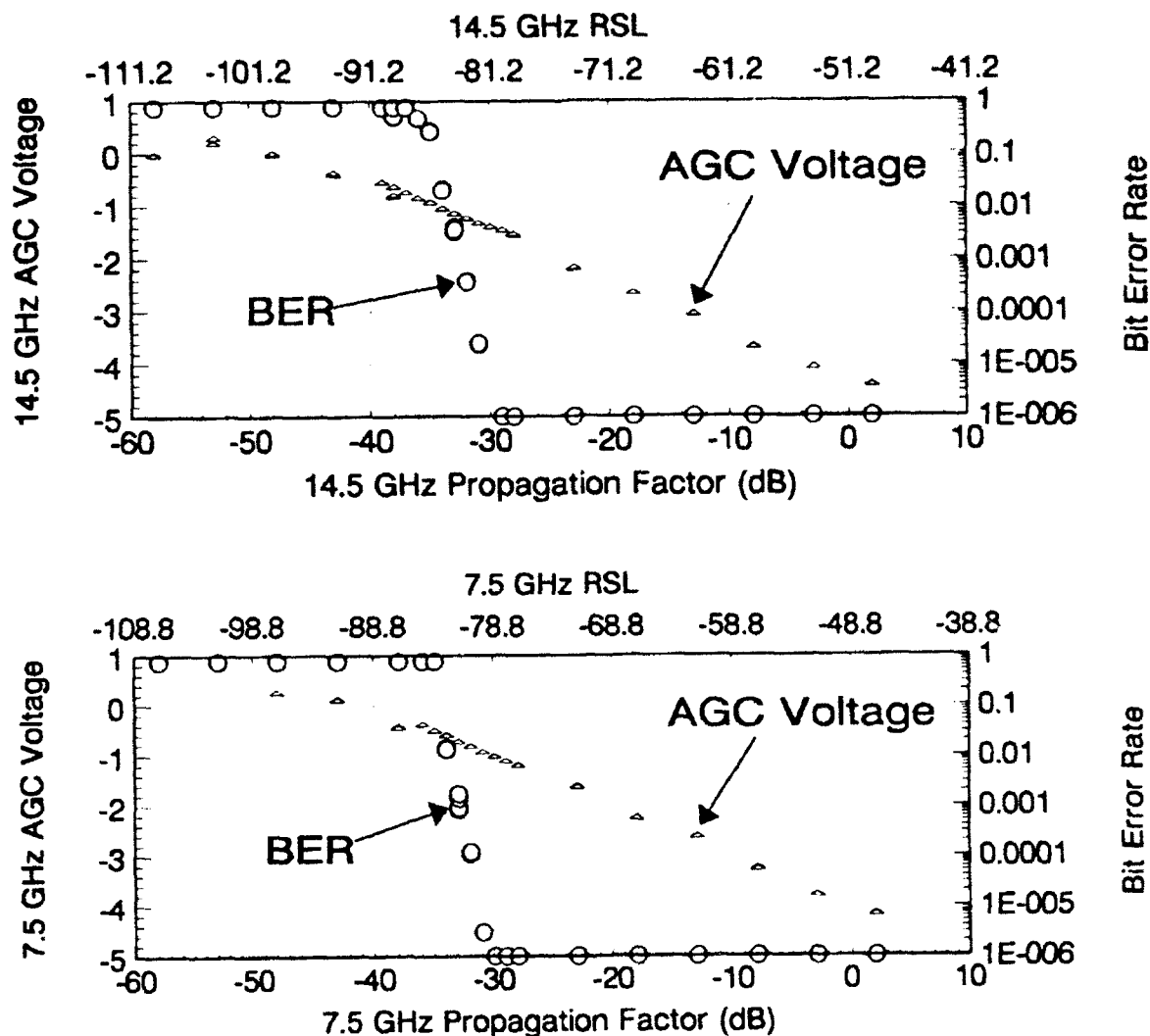
Figure 7. Receiver calibration curves.

ANTENNA TESTING

With transmit and receive sites for EDCOM being well beyond line of sight, and with the strong possibility of a bursty and rapidly fading channel, antenna alignment methods that utilize sighting the other antenna, or varying the antenna position to find the highest field strength, are not usable; therefore, antenna alignments must be done by precise optical alignments (using a theodolite across the face of the antenna) in conjunction with geographical surveys. This makes it necessary to ensure that the peak antenna field strength pattern is normal to a line across the face of the antenna. Additionally, antenna peak gain is required for use in link equations.

All antennas were assembled and tested on an antenna range. Horizontal and vertical patterns were obtained using standard gain horns for reference. Optical alignments were obtained using a theodolite across the face of each antenna. Table 5 provides the peak

11

antenna gain, both the vertical and horizontal half-power beamwidths, and the vertical and horizontal alignment errors. The alignment error is the difference between pattern center and optical alignment center.

Table 5. Antenna performance.

| Antenna No./ Frequency | Peak Gain (dB) | Vertical | | Horizontal | |
		Half-Power Beamwidth (deg)	Alignment Error (deg)	Half-Power Beamwidth (deg)	Alignment Error (deg)
315/7.5 GHz	34.8	2.4	< 0.5	2.7	< 0.2
316/7.5 GHz	36.8	2.7	< 0.5	2.6	< 0.5
001/14.5 GHz	41.6	1.2	< 0.5	1.4	< 0.5
002/14.5 GHz	40.1	1.4	< 0.5	2.0	< 0.25

LOSS CALCULATIONS

System "constants" include power transmitted (P_T), antenna gains (G_T and G_R), insertion losses (IL). All of the system constants except the insertion losses (combined losses due to the coaxial cable between the transmitter and the transmitting antenna and the coaxial cable between the receiver and the receiving antenna) are determined experimentally as described in the preceding sections. The insertion losses of these cables are determined from manufacturer's data. The system constants are listed in table 6.

Table 6. Summary of system constants for 7.5-GHz and 14.5-GHz links.

Quantity	Definition	7.5 GHz	14.5 GHz
P_T	Transmitted Power (dBm)	29.4	23.2
G_T	Transmit Antenna Gain (dB)	34.8	41.6
G_R	Receive Antenna Gain (dB)	36.8	40.1
$PL_{FREE-SPACE}$	Free Space Path Loss (dB)	148.3	154.1
IL	Insertion Loss (dB)	1.2	2.0

A useful convention for the path loss (L) at beyond line-of-sight ranges is to reference L to the free-space path loss (L_{FS}) by defining the propagation factor (PF) as the propagation loss minus the free space propagation loss as follows:

$$PF = L - L_{FS} \tag{4}$$

where L_{FS} is determined by

$$L_{FS} = 32.45 + 20\log(d) + 20\log(f) \tag{5}$$

12

for distance d, in kilometers, and frequency f, in megahertz. For a one-way transmission system, signal power at the receiver is

$$P_R = P_T + G_T - L - IL + G_R \tag{6}$$

Rewriting and using equation (4) the following is obtained:

$$PF = P_T + G_T - P_R - IL + G_R - L_{FS} \tag{7}$$

AGC voltage, calibrated to power at the receiver P_R (equations [2] and [3]), is continuously measured during link operation thus completing the information required to compute the propagation factor PF. Equations (8) and (9) are obtained for the propagation factors of 7.5 GHz and 14.5 GHz, respectively, by inserting the quantities of table 4 into equation (6).

$$PF_{7.5} = -48.5 - RSL_{7.5-GHz} \tag{8}$$

$$PF_{14.5} = -51.2 - RSL_{14.5-GHz} \tag{9}$$

RESULTS

Measurements began in late January 1992 and continued until May 1992. Eight measurement periods, totaling 89 days of operation and over 15,000 observations, were completed during this time. Table 7 lists the continuous measurement periods.

Table 7. Dates of measurements in 1992.

Start		End		
Date	Time	Date	Time	Days
22 Jan.	1100	24 Jan.	0800	1.8
27 Jan.	0800	27 Jan.	2359	0.7
28 Jan.	0700	19 Feb.	2359	22.7
22 Feb.	0001	26 Feb.	2359	5.0
29 Feb.	0001	03 Mar	1057	3.4
11 Mar.	0001	27 Apr.	0800	47.3
05 May	0700	08 May	1300	2.8
11 May	1726	17 May	0046	5.3

One-way transmission-path data are analyzed by comparing observed propagation factors to expected propagation factors for the observed surface meteorology. The evaporation duct M profile is calculated from surface meteorological parameters of wind speed, air temperature, relative humidity, and sea temperature. All meteorological parameters, except ambient sea-water temperature, are averages of those measured at the transmit and receive site. Only the receive site is instrumented for measuring sea-water temperature. Expected propagation factors are obtained from MLAYER for a given evaporation duct height δ. The refractivity profile, as measured in M-units from the air and sea interface up to the evaporation duct height, is determined by the Jeske (1971) method. A "Standard Atmosphere" refractivity profile is assumed to exist above the evaporation duct height.

Nonstandard atmospheric refractivity profiles may produce signal enhancements that are tens of dB's above the signal levels experienced when the refractivity profile is that of the evaporation duct coupled with a standard profile. Figures 8 and 9 provide height versus M-unit profiles for 86 atmospheric soundings obtained at Montgomery field, San Diego, California, in the period beginning 28 January 1992 and ending 25 March 1992. Each of these soundings is labeled STD, SBD, ELEV, or OTHER to indicate if the M-unit profile is representative of a standard atmosphere (STD), if it is associated with a surface-based duct (SBD), if it is an elevated duct (ELEV), or if the profile does not clearly fall into these categories, hence (OTHER). These soundings are used to explain the behavior of the received signal levels and to classify received signal levels, based on whether the atmosphere was standard or nonstandard. Because of the very great effect that the vertical refractivity structure above the evaporation duct height plays upon signal strengths, the time series displayed, beginning with figure 11, were chosen as they coincide with periods for which atmospheric soundings were obtained.
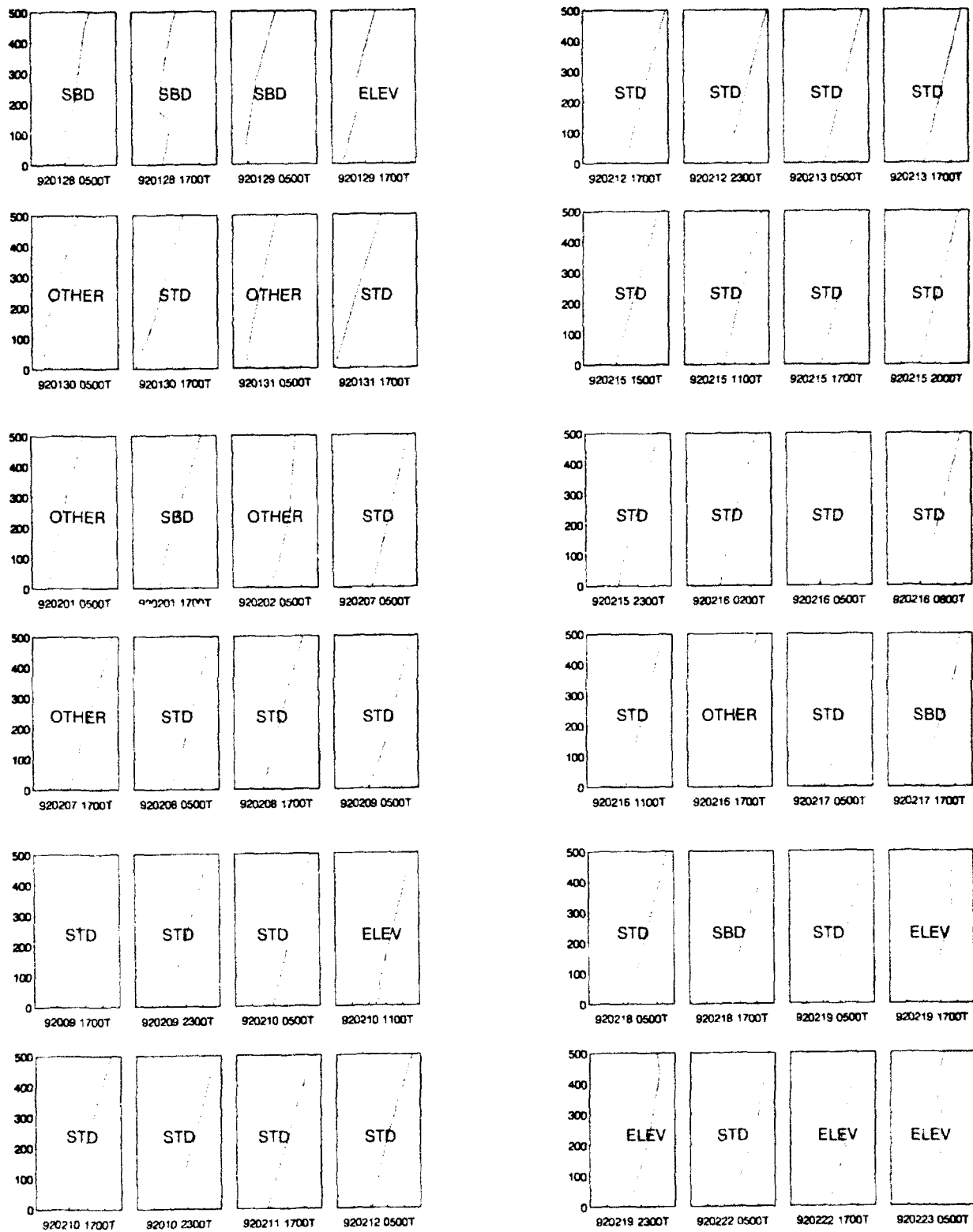
14

Figure 8. Montgomery field atmospheric soundings from 8 January 1992 through 23 February 1992. Each abscissa division is 25 *M*-units.
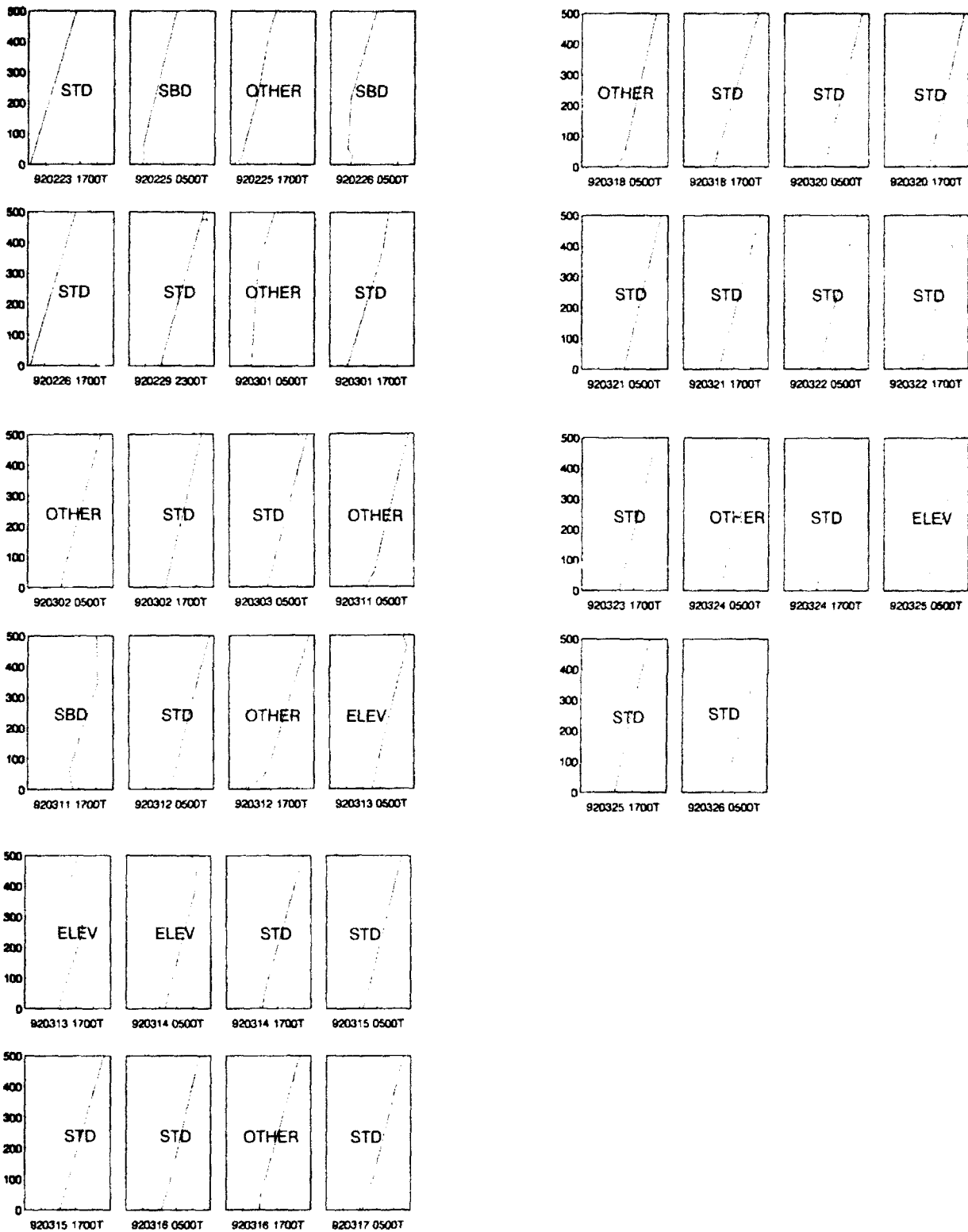
Figure 9. Montgomery field atmospheric soundings from 23 February 1992 through 26 March 1992. Each abscissa division is 25 *M*-units.

SOUTHERN CALIFORNIA COASTAL CLIMATE

The EDCOM experiment was conducted in the southern California coastal area. In this area, the coastline runs northwest/southeast. Data from climatic studies (Patterson, 1987) indicate that the most common wind flows north-northwest in the winter and shifts to west-northwest in the spring. This flow is nearly parallel to the coast. Within a few miles to many from the coast, sea breeze effects override the prevailing surface wind. The normal diurnal cycle is as follows: In the morning, the air is still, or blowing off-shore; around noon, the land mass has heated enough to provide the driving head for the sea breeze; sometime before dark, the sea breeze reaches its maximum velocity (typically 6 − 14 knots). When the sea breeze is weak, it abates shortly after dark; when strong, the sea breeze may persist until late in the evening. Sometime in the morning, the land breeze begins as the land cools below the temperature of the ocean. As the magnitude of the temperature differential between the land and the ocean is less than that experienced with the afternoon sea breeze, the land breeze is usually weaker than the sea breeze, seldom exceeding 10 knots.

Many other factors come into play. Often in winter there tends to be a high pressure zone over the Rocky Mountains. This high pressure tends to drive the continental air mass over the ocean in the southern California coastal area. The result is cool dry air over the ocean in the coastal area. This flow is in opposite direction to the sea breeze, so while the sea breeze almost inevitably does develop, it is of reduced magnitude and does not persist long into the evening. Frequently in the summer, there exists a high pressure zone over the Pacific Ocean and a low pressure system centered over the Rocky Mountain region. This pressure differential contributes to the shift of the prevailing winds from being evenly distributed about the northwestern half of the compass rose to being almost exclusively from west to northwest. Longer days and higher inland temperatures let the sea breeze fully develop, resulting in higher wind velocities persisting longer into the evening.

LONG-TERM TIME SERIES

Figure 10 is a legend for the time series presented in figures 11 through 22. The bottom four plots of figures 11 through 22 include relative humidity, wind direction, wind speed and the resulting evaporation duct height. Air temperature and sea temperature are also used in the computation of the evaporation duct height, but are not shown, as they have less of a contribution than the wind speed and humidity in the context of the EDCOM experiment. Surface-based duct height (based upon atmospheric soundings) is shown on the same plot as the evaporation duct height. Predicted and measured propagation factors at 7.5 and 14.5 GHz are shown in the top two plots of these figures. The periods of time covered in figures 11 through 22 comprise approximately half of the measurements recorded during the EDCOM experiment. The availability of atmospheric soundings determined the periods chosen.
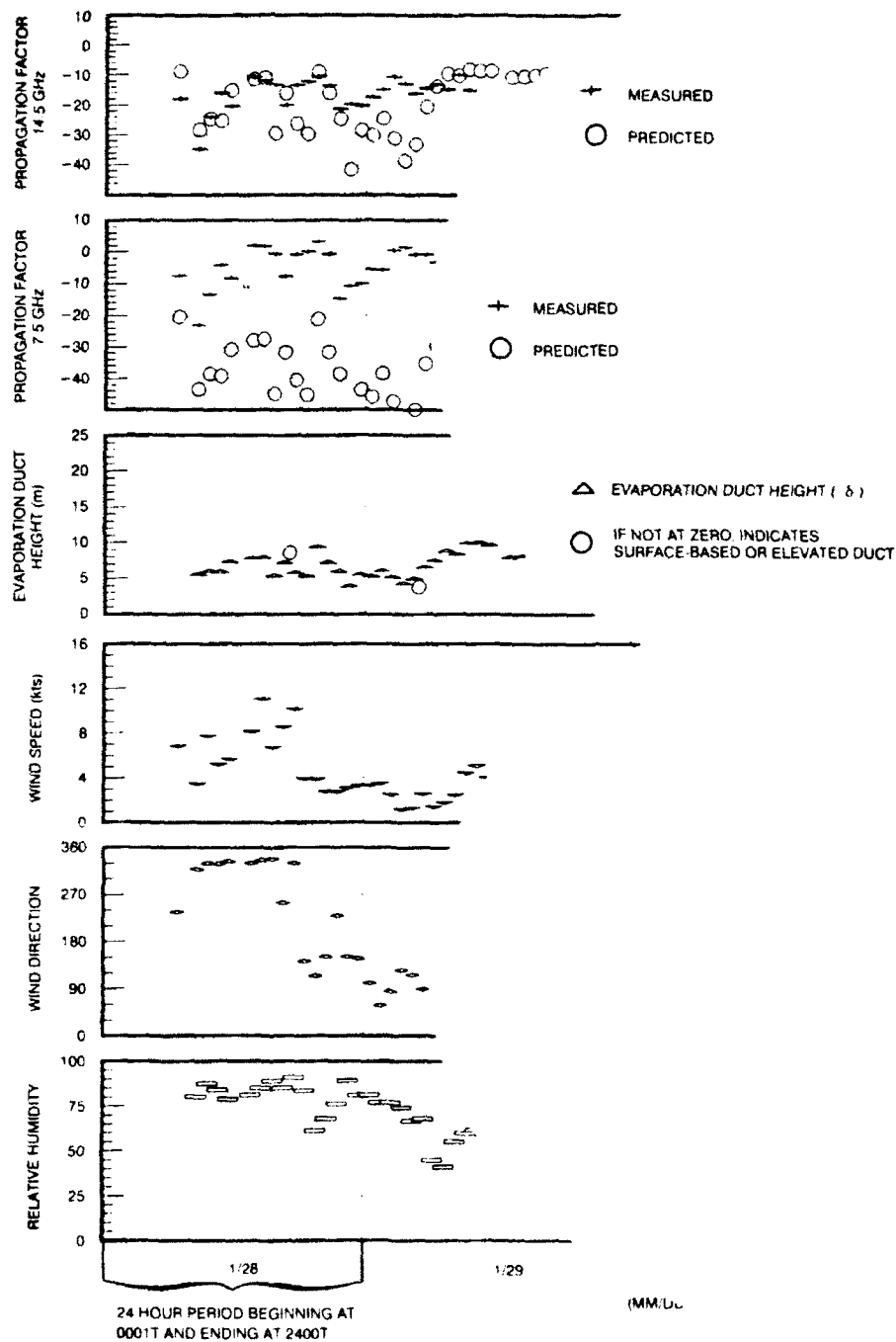
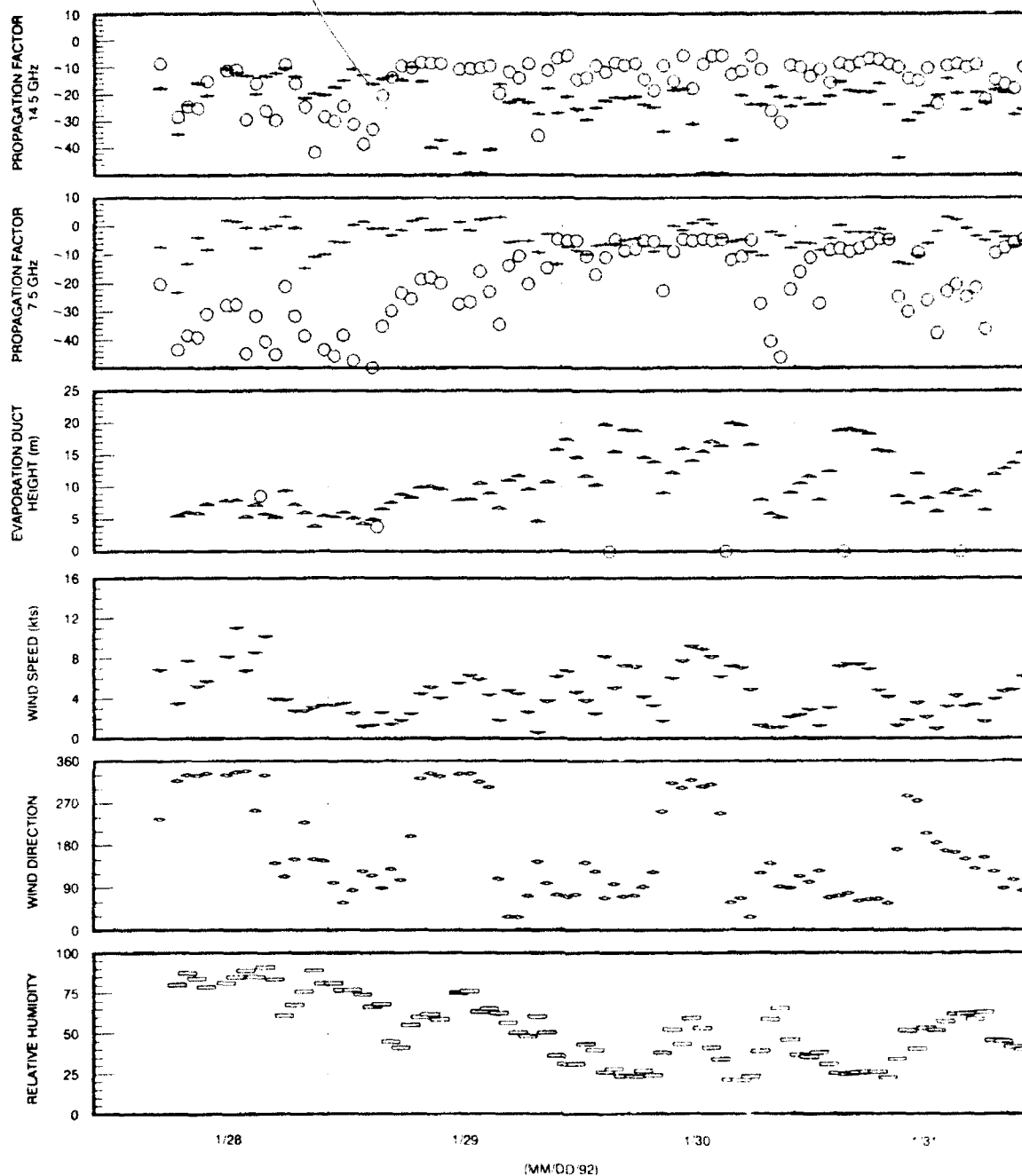Figure 10. Legend for time series in figures 11 through 22.

18

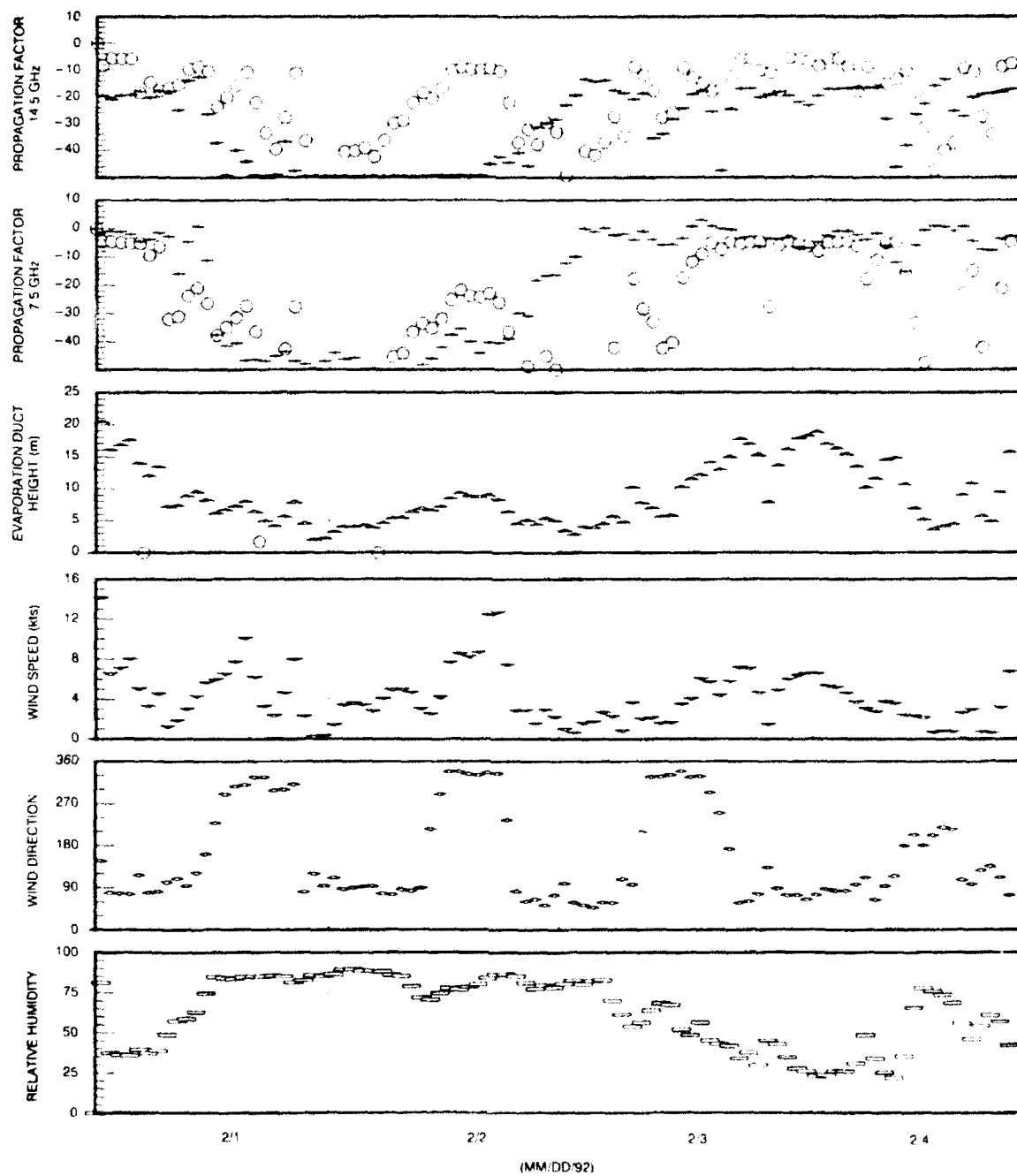Figure 11. Time series covering 28 January 1992 through 31 January 1992.

Figure 12. Time series covering 1 February 1992 through 4 February 1992.
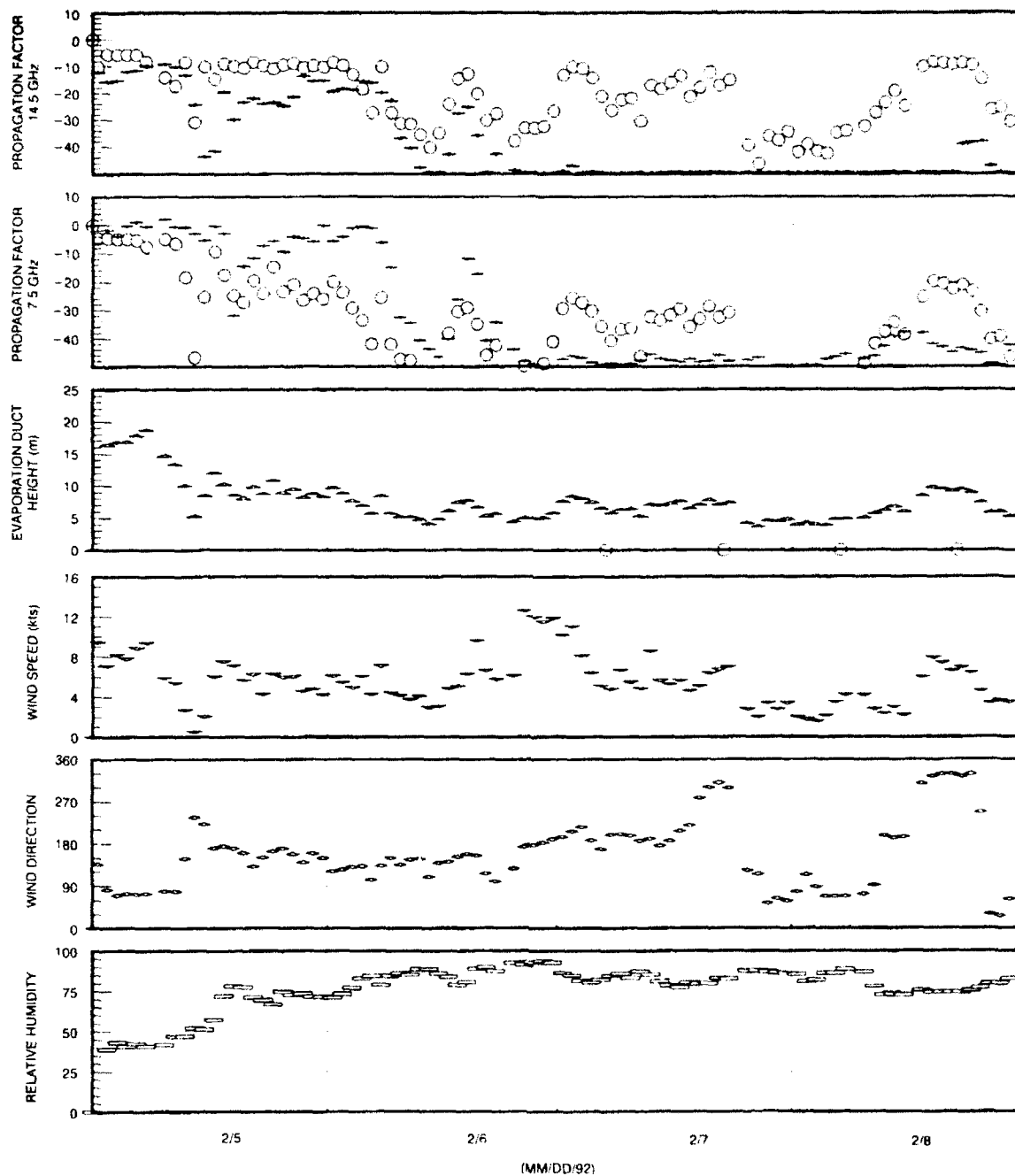
Figure 13. Time series covering 5 February 1992 through 8 February 1992.

Figure 14. Time series covering 9 February 1992 through 12 February 1992.
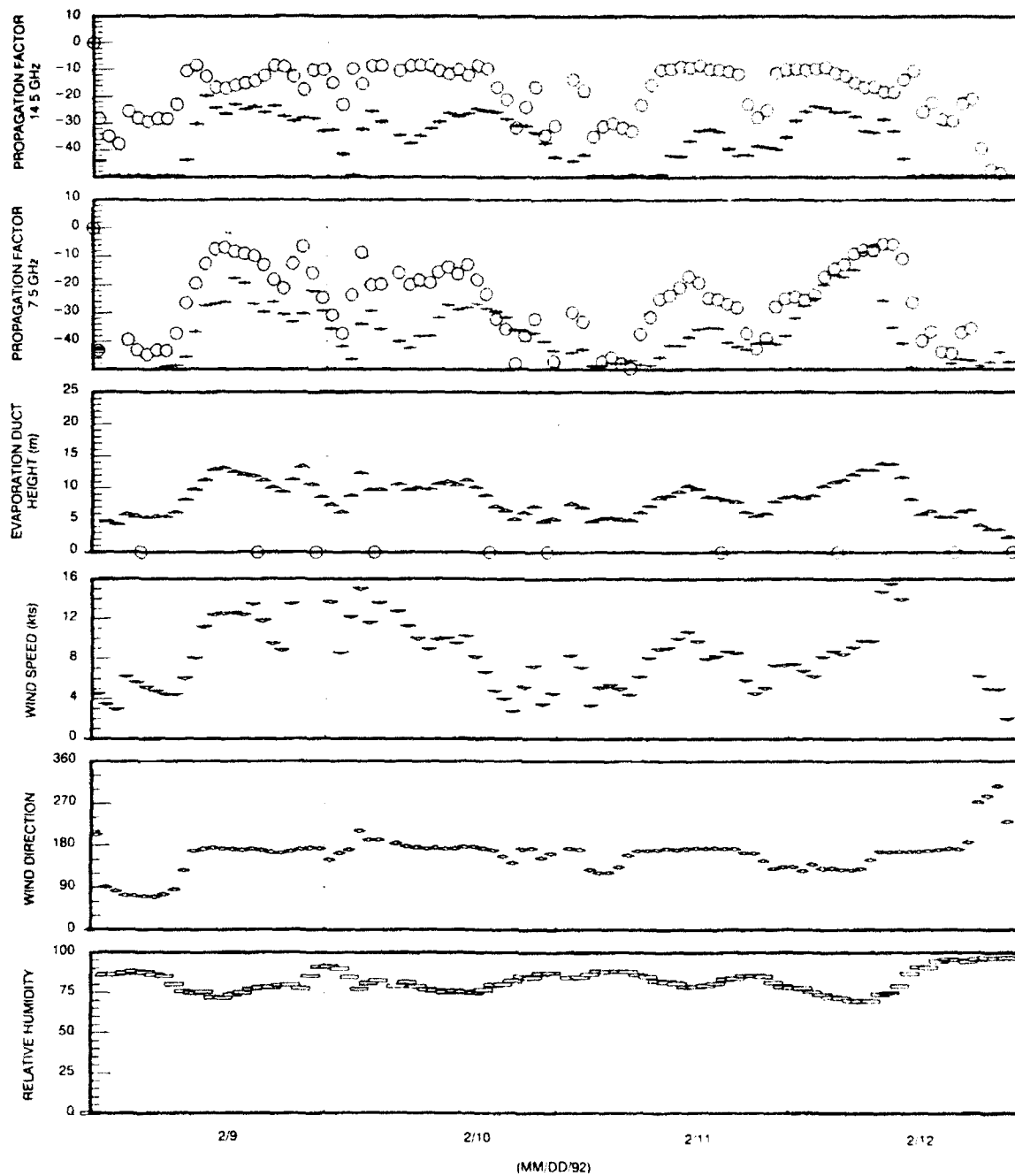
Figure 15. Time series covering 13 February 1992 through 16 February 1992.

23

Figure 16. Time series covering 17 February 1992 through 20 February 1992.

24
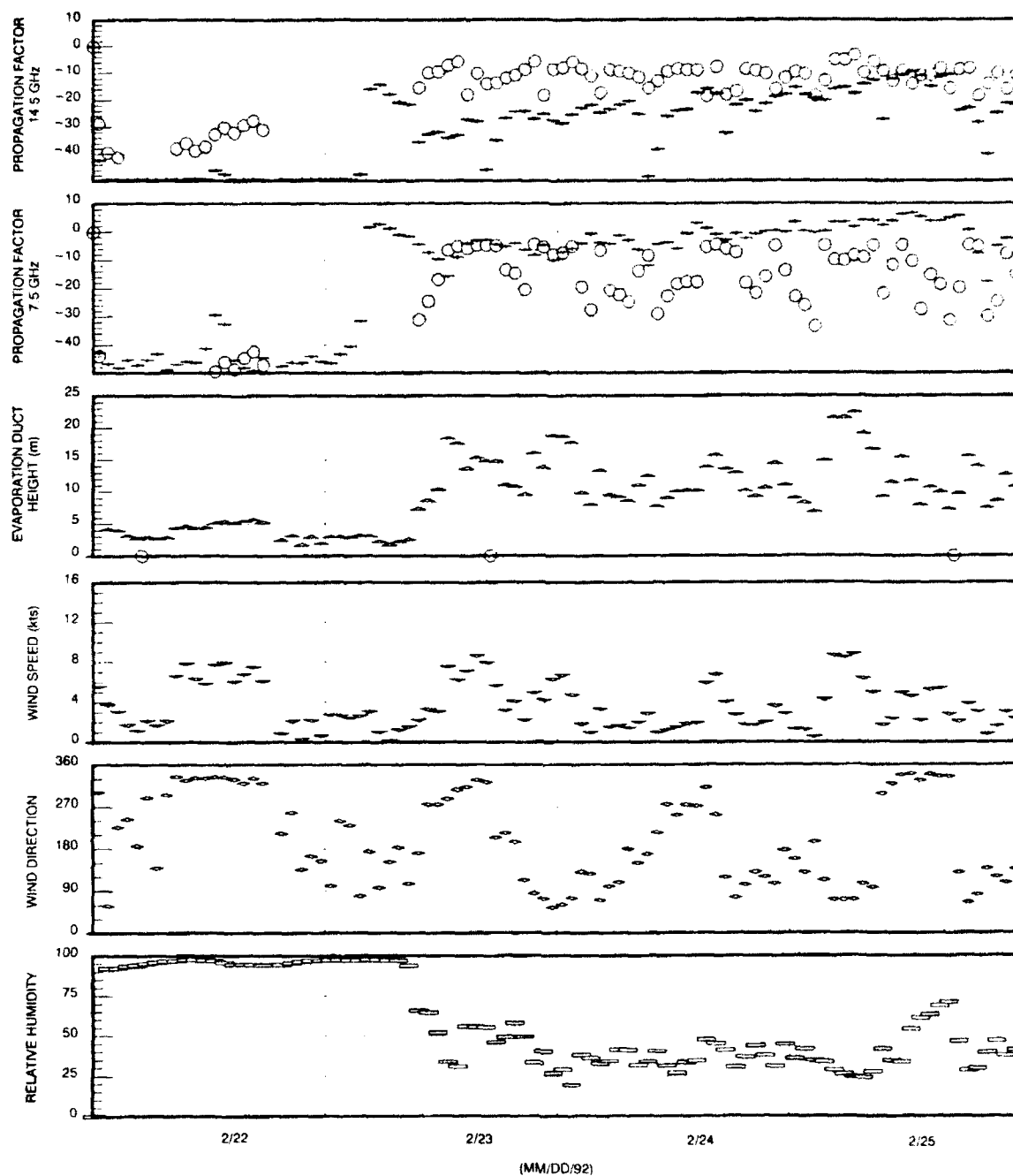
Figure 17. Time series covering 22 February 1992 through 25 February 1992.

Figure 18. Time series covering 29 February 1992 through 3 March 1992.

Figure 19. Time series covering 11 March 1992 through 14 March 1992.

27

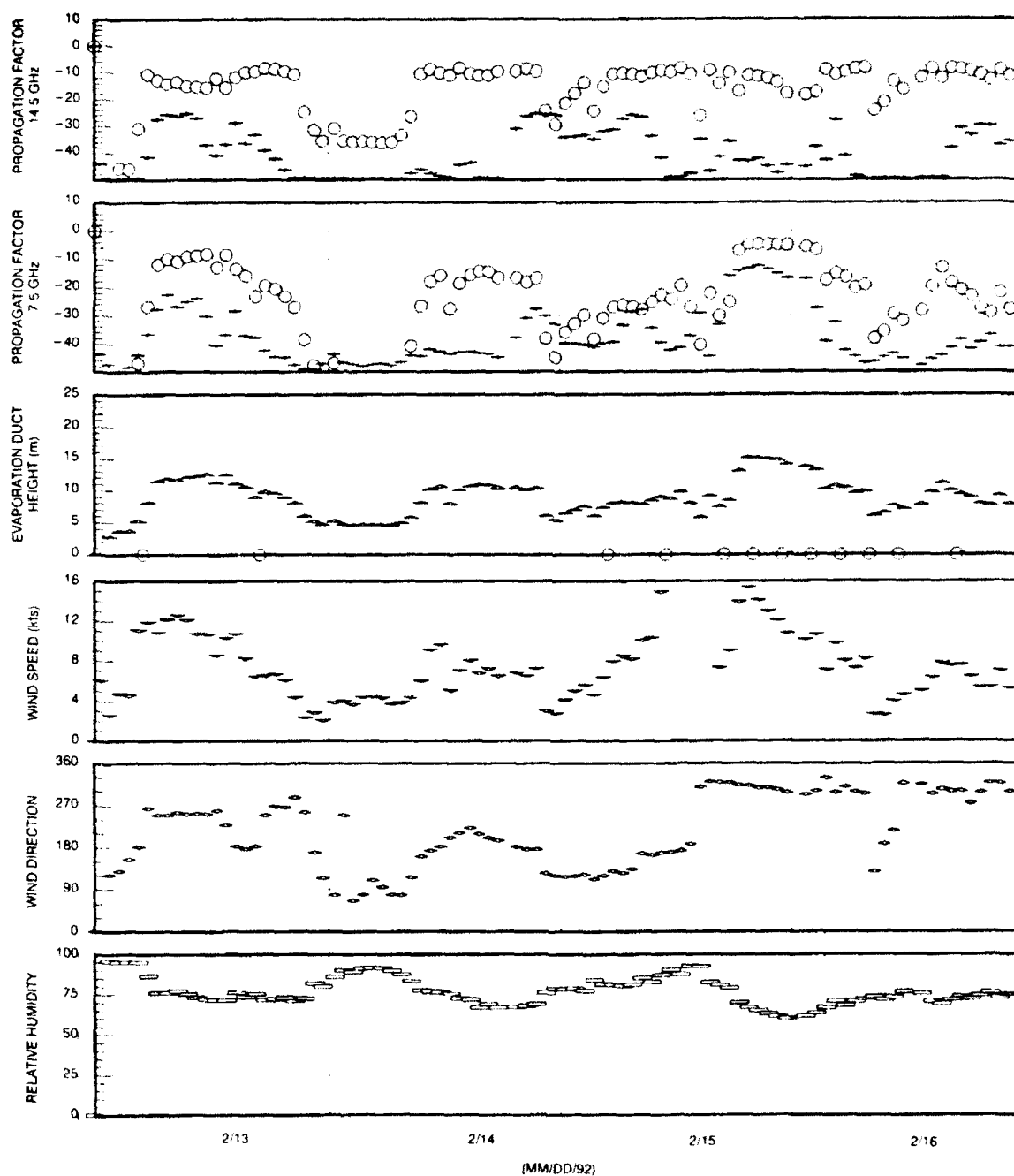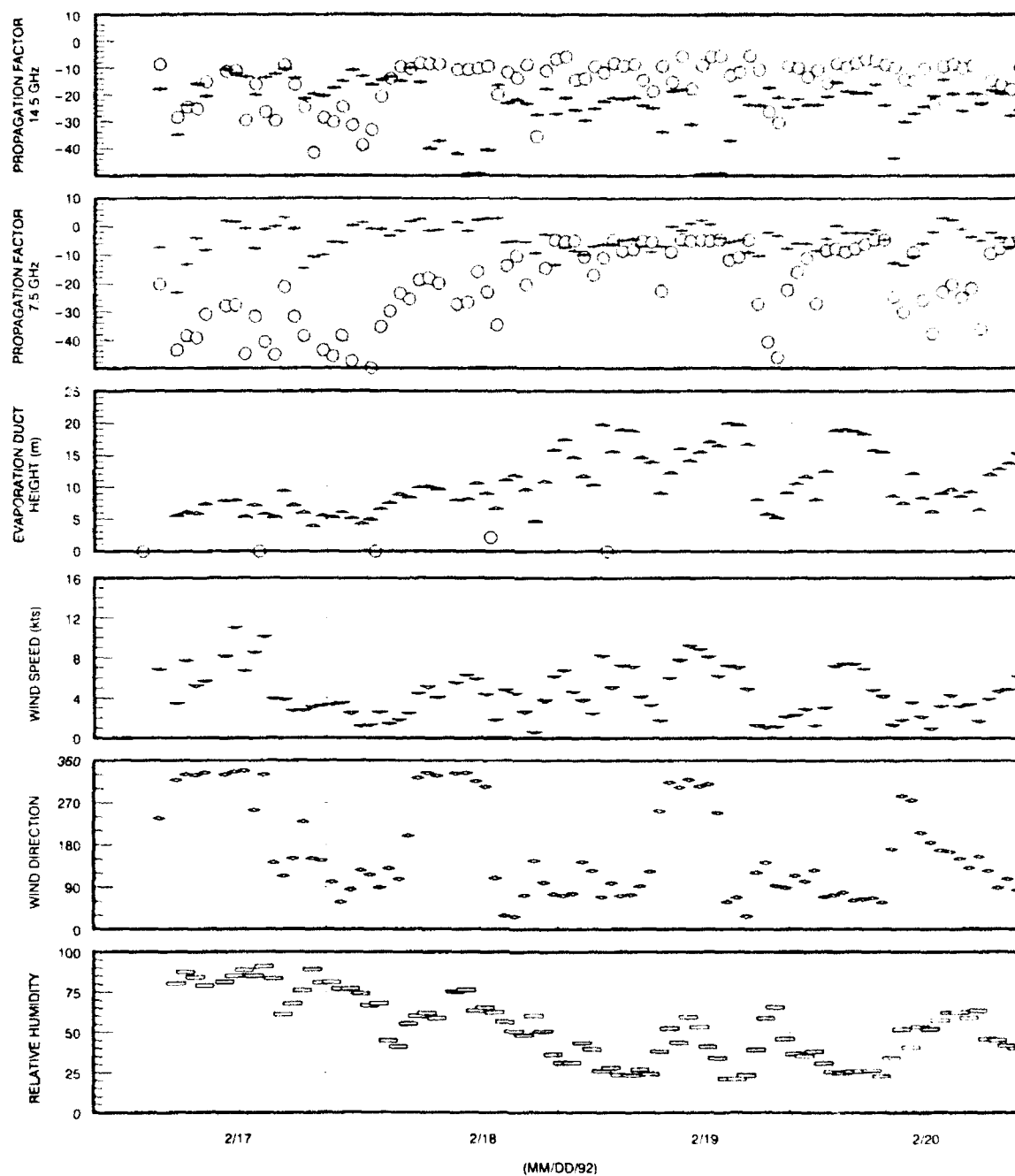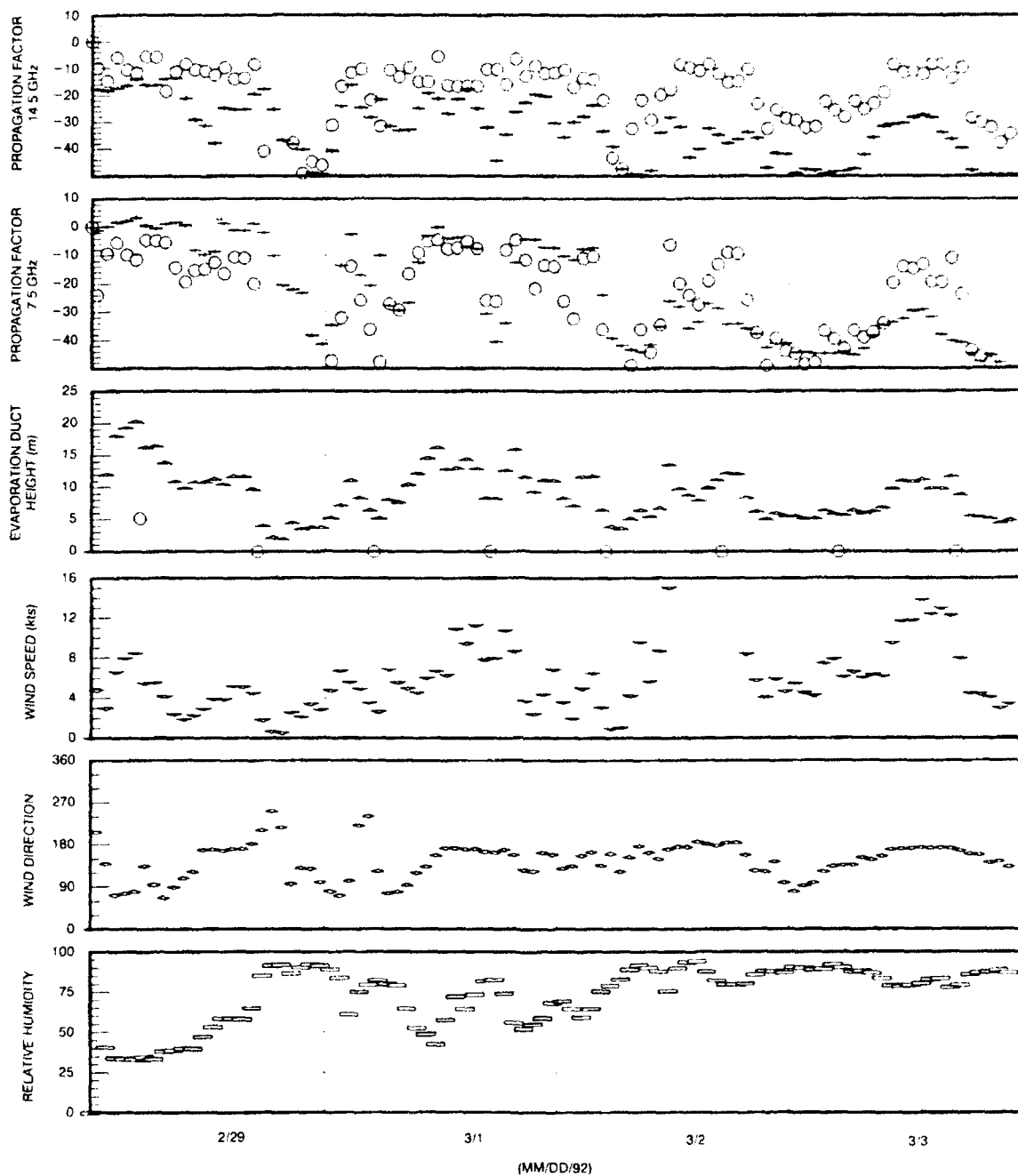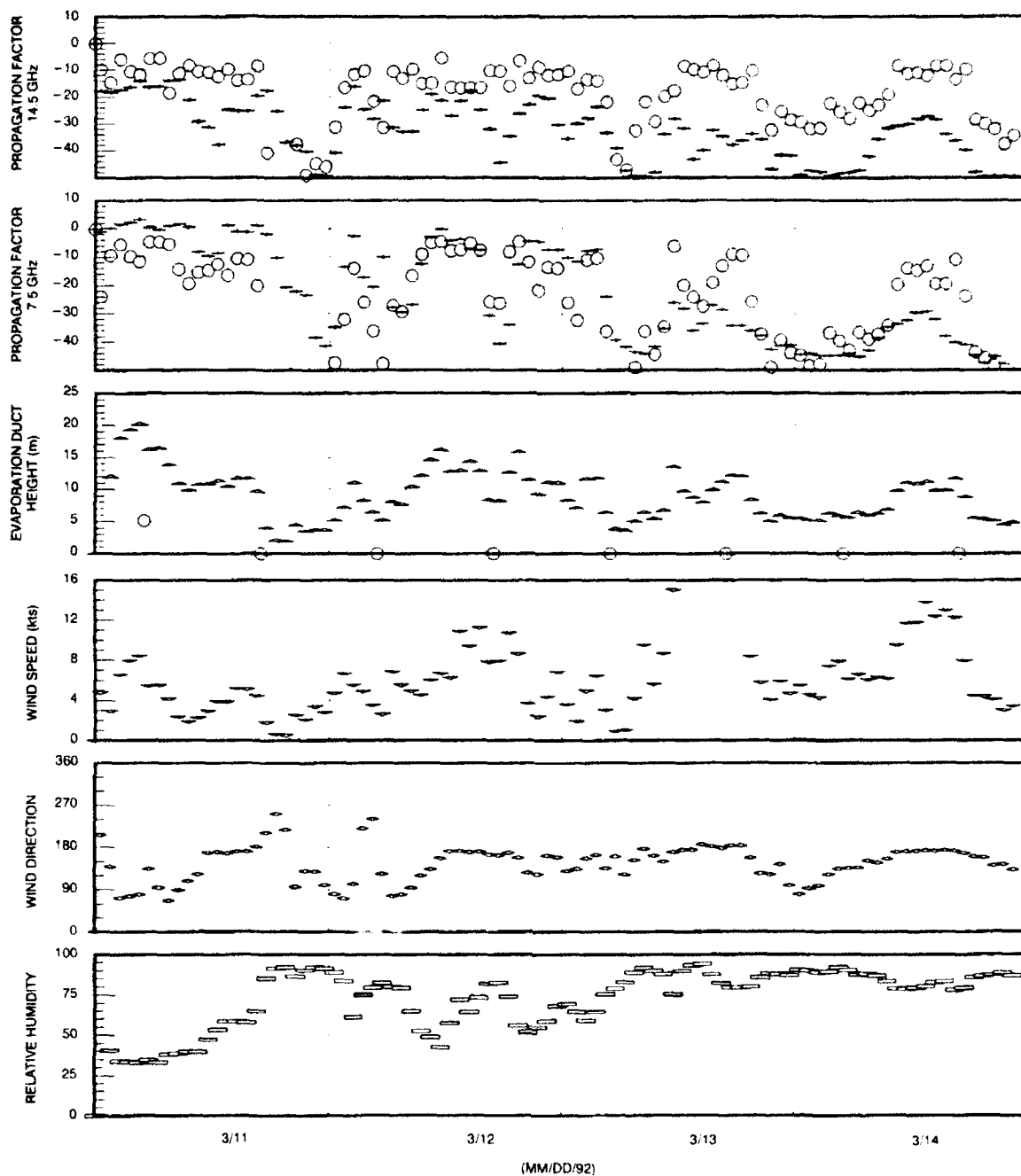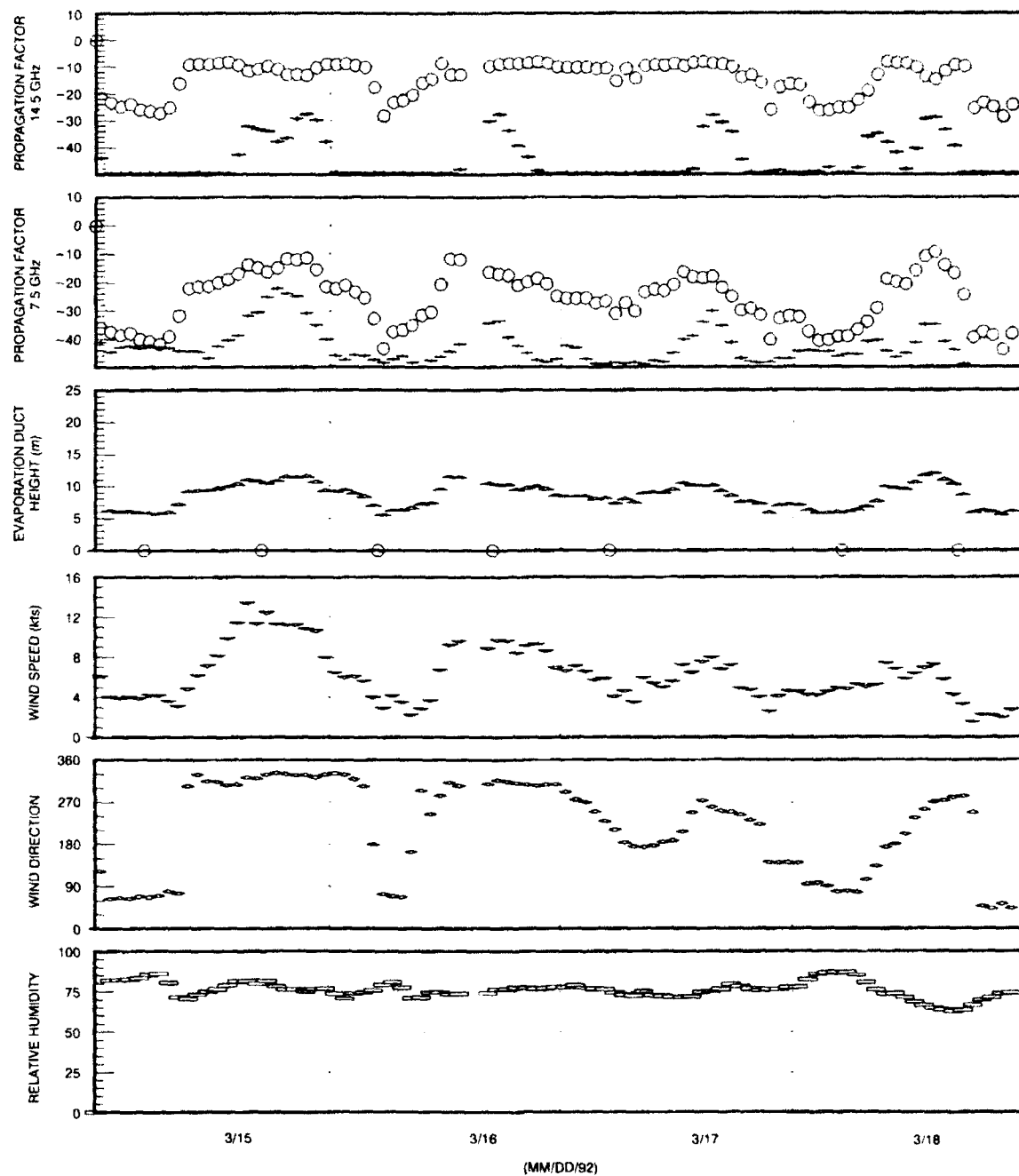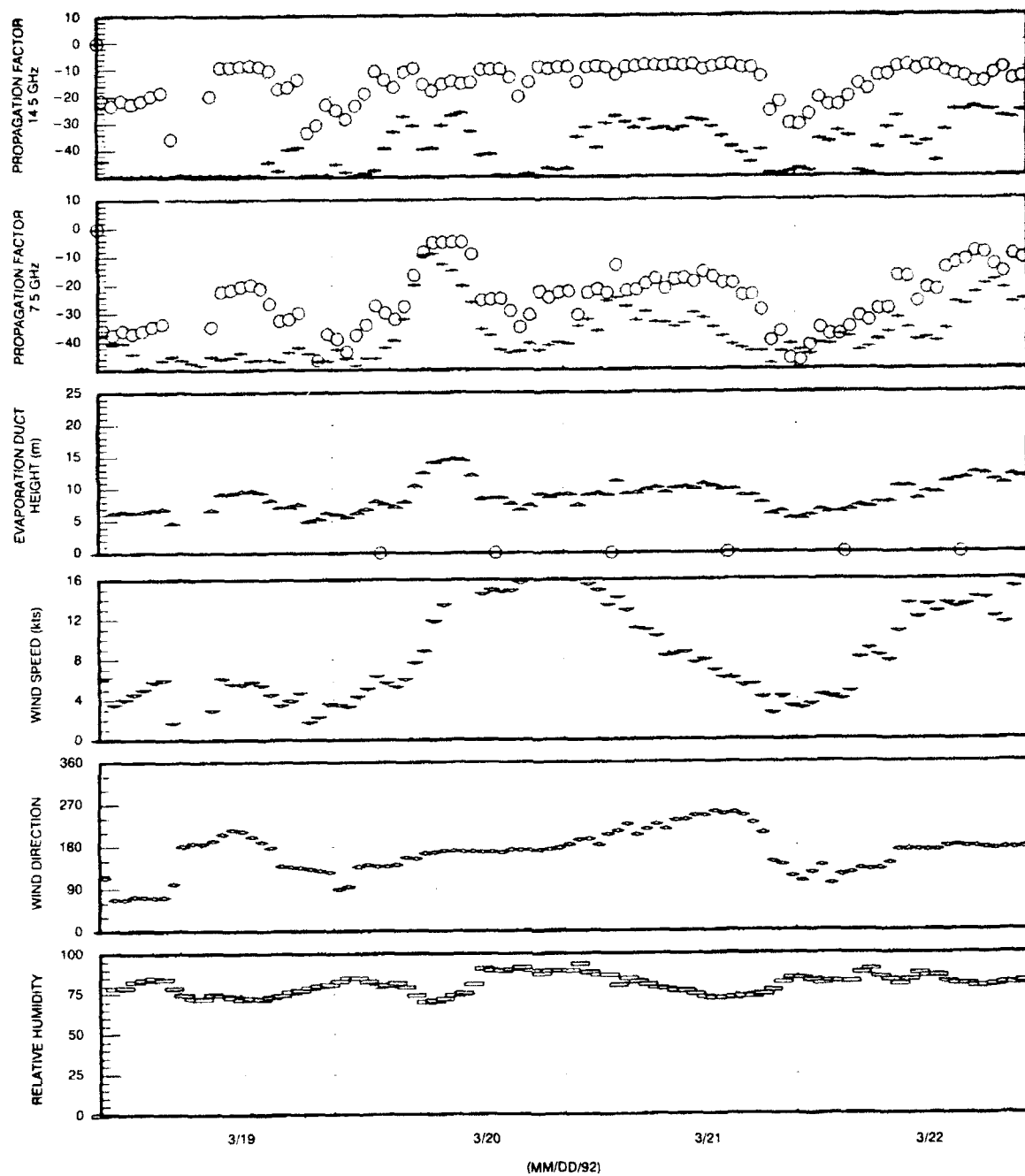Figure 20. Time series covering 15 March 1992 through 18 March 1992.

28

Figure 21. Time series covering 19 March 1992 through 22 March 1992.
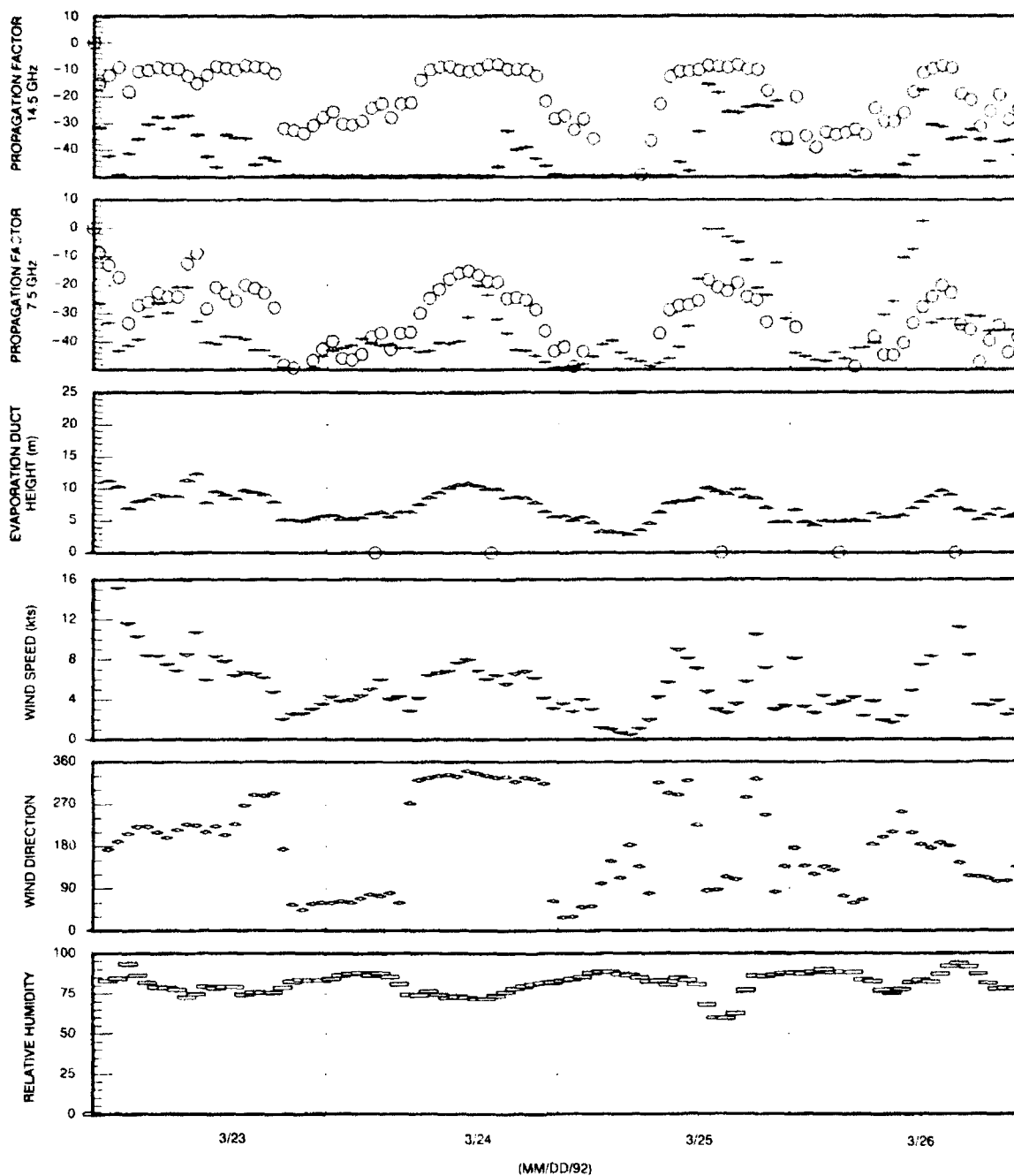
29

Figure 22. Time series covering 23 March 1992 through 26 March 1992.

Figure 11 covers the period beginning at 0800 (local) on 28 January 1992, continuing up through midnight on the 31 January 1992. The dominant factor in this time period is the presence of nonstandard refractivity profiles above the evaporation duct. From figure 8, it is seen that the soundings of 0500 and 1700 on 28 January, and 0500 on 29 January, indicate surface-based ducts. Soundings at 0500 on 30 and 31 January, while not qualifying as surface-based ducts (they have slightly positive slopes), are super-refractive profiles. Only one of eight atmospheric soundings in this period indicates a standard, or nearly standard, refractivity profile. During this period, propagation factors seem independent of evaporation duct height, with measured values staying between −10 and +5 dB at 7.5 GHz, and between −30 and −10 dB at 14.5 GHz. It will be seen later, that when there is a standard refractivity profile, measured propagation factors are 10 dB (or more) below predicted values at 7.5 GHz, and 20 dB (or more) below predicted values at 14.5 GHz.

Meteorological trends observed during this period bear examination. The diurnal pattern with wind direction is immediately clear. The wind blows from roughly 090 degrees true from 1800 until 0800 the next morning. Then from 0800 until 1800, the wind is blowing from the north or the west. On 28 January, the humidity is quite high, which suggests the source of the air mass is from the ocean. From midday on 29 January until the end of the period, the humidity is generally less than 60%, suggesting continental air flow. Wind speeds are moderate. It is not until midday on the 29th that the evaporation duct height exceeds 10 meters.

A transition in this period of time is from what might be described as *Normal* conditions (70% or greater humidity, conditions dominated by onshore air mass flow) to what will be referred to as *Santa Ana* conditions. During *Santa Ana* conditions, the bulk of the air mass flow in the southern California area is offshore: that is, the source of the air mass over the water near shore is from the continent as opposed to the ocean. This very dry air produces evaporation duct heights ranging from 10 to 20 m. As two of the last three atmospheric soundings in this period indicated nonstandard profiles, the very high signal levels are not necessarily attributable to the high evaporation duct heights.

Figure 12 is a 4-day period beginning on 1 February 1992 at 0000 that begins with *Santa Ana* conditions: The wind is directly from the east and the relataive humidity is quite low (35%). The evaporation duct height is correspondingly high, reflecting the large vertical distance required to go from saturation conditions at the air-to-sea interface to the low ambient humidity of the air mass. During this period, the measured propagation factor at 14.5 GHz is around 10 dB less than predicted value, and the measured propagation factor at 7.5 GHz is 5 to 15 dB above predicted values. Two atmospheric soundings are taken that day, one at 0500 and the other at 1700 (local time). The first sounding does not indicate a surface-based duct. However, in the first 50 m, the refractivity profile is less steep than the standard profile. The sounding at 1700 indicates a 35-m surface-based duct. In the period between both soundings, the predicted and measured propagation factors drop, and the difference between them increases, as a transition is made from *Santa Ana* to normal conditions where any signal enhancement is due to the evaporation duct. The conditions at 1500 include an onshore flow and a light wind ranging from 4 to 8 knots, blowing from the northwest. Humidity is high, greater than 80%, and the evaporation duct height is 8 m, or less.

31

By 1500 on 2 February, the measured propagation factor at 14.5 GHz is 20 to 25 dB less than the predicted value; and at 7.5 GHz, the measured values are 10 to 15 dB below predicted values.

Late afternoon on 2 February, it appears that the atmospheric structure above the evaporation duct is nonstandard. By 0100 on 3 February, measured signal levels are 25 dB, or more, above predicted levels at 14.5 GHz, and 40 dB above predicted levels at 7.5 GHz. The wind varies from 350 to 100 degrees true and, as the humidity is dropping, it appears there is a continental air flow. From 1000 until 1500 on 4 February, the humidity begins to rise again, and the wind is from 270 degrees true (seaward), reflecting some sea breeze effects, but the wind velocity never exceeds 7 knots. The winds shift is out of the south, and then from the west again, to provide *Santa Ana* conditions. During this period of time, propagation factors at 7.5 GHz remain very high, but at 14.5 GHz, they vary over a 40-dB range. From 2 to 7 February, atmospheric soundings are not available, so it is only suspected that nonstandard refractivity profiles are the cause of the high propagation factors experienced during this period.

Figure 13, covering the period 5 to 8 February, begins with 40% relative humidity and winds at 8 knots from the east, that is to say, *Santa Ana* conditions. Propagation factors are in line with those associated with surface based ducts. By 6 February, though it appears that a transition has been made to evaporative ducting conditions, those conditions where the refractivity profile is above the evaporation duct, are standard, or nearly so. Three of four soundings on 7 and 8 February indicate standard profiles; the other is super-refractive, below 60 meters. These are the conditions that the EDCOM experiment was designed for: conditions where the evaporation duct is the dominant mode of propagation. On 8 and 9 February, the signal levels are frequently below detection level. It is only on the 8th of February, when the evaporation duct reaches approximately 8 m, that the propagation factor at 14.5 GHz rises above −40 dB. It should be also noted that on 8 February, the propagation factor at 14.5 GHz lags the predicted value by a few hours.

The measurement period from 9 to 16 February is shown in figures 14 and 15. All atmospheric soundings from the period in figure 8 are standard or nearly so. The humidity is relatively high, the wind speeds vary from 4 to 16 knots, and the evaporation duct heights vary accordingly from 5 to 15 meters. For the duration of this period, measured signal strengths follow predicted levels and are about 15 to 35 dB low at 14.5 GHz and 10 to 20 dB low at 7.5 GHz. Note that five soundings were taken each day on 15 and 16 February. All soundings, except the very last, indicate standard profiles. These standard profiles consistently increase the confidence that for this period of time the evaporation duct is the dominant mode of propagation.

Figure 16 covers the period of 17 to 19 February inclusively (the experiment was off-line on the 20th.) Measured propagation factors follow the predicted values as they did in figures 14 and 15. However, atmospheric soundings at 1700 on 17 and 18 February show 30- and 45-m surface-based ducts, respectively. It has been observed that surface-based duct profiles are usually associated with elevated propagation factors. This counter example illustrates the variability inherent when applying single geographical point measurements of the atmospheric refractivity to an entire transmission path. Examining the

meteorological parameters, it is seen that the humidity stays generally above 75%, and the wind is mostly from the north. Sea breeze effects are seen in the form of increasing wind velocities and more westerly wind direction in the afternoon.

Figure 17 covers the period 22 to 25 February inclusively. From 0001 on 22 February until 0800 on 23 February, humidity is 90% or greater, and the evaporation duct heights are 6 m, or less. The first of the two atmospheric refractivity profiles is standard. The second profile (1700) indicates an elevated duct that does not appear to have, and should not have, a large effect on signal strengths. Two of the four soundings taken on 23 and 24 February show nonstandard profiles. The propagation factors are very high, typical of conditions seen during surface-based ducts or low elevated ducts.

From the soundings and time series discussed so far, the following three general observations are made and are borne out by the remainder of the test data:

- During periods of *onshore* flow with a *standard* vertical refractivity profile, propagation factors at both 14.5 GHz and 7.5 GHz follow predicted values; however, they are typically around 25 dB and 15 dB less than predicted values, respectively.

- Periods of *offshore* flow accompanied by low relative humidity give rise to signal levels that are near predicted values at 14.5 GHz and exceed predicted values at 7.5 GHz.

- If some of the soundings in a period of a few days show surface-based or elevated ducts, then often, that entire period may have signal levels that are near predicted values at 14.5 GHz and exceed predicted values at 7.5 GHz.

Figures 18 through 22 cover those periods between 29 February and 26 March when the system was operational and atmospheric soundings were obtained. The figures provide further examples of the general observations noted. Again, figures 8 and 9 provide associated soundings.

CUMULATIVE DISTRIBUTIONS

Distributions of measured propagation factor, and the propagation factor predicted by climatological and meteorological measurements, are shown in figure 23. The curve labeled *Climatology* is the distribution of propagation factor predicted by *MLAYER* based upon historical distributions for evaporation duct heights in the southern California area. The curve labeled *Predicted* is the distribution of propagation factors predicted by *MLAYER* based upon meteorological observations at the receive site (predicted distributions based upon transmit site are nearly identical). The curve labeled *Measured* is the distribution of actual propagation factor data. At 14.5 GHz, the 40% point on the ordinant of the *Measured* curve is offset 27 dB from *Climatology* and *Predicted* curves. Similarly, the propagation factor corresponding to 10^{-6} BER is -30 dB, and both *Climatology* and *Predicted* propagation factors exceed this value 81% of time, while the *Measured* propagation factor exceeds this value 27% of time.
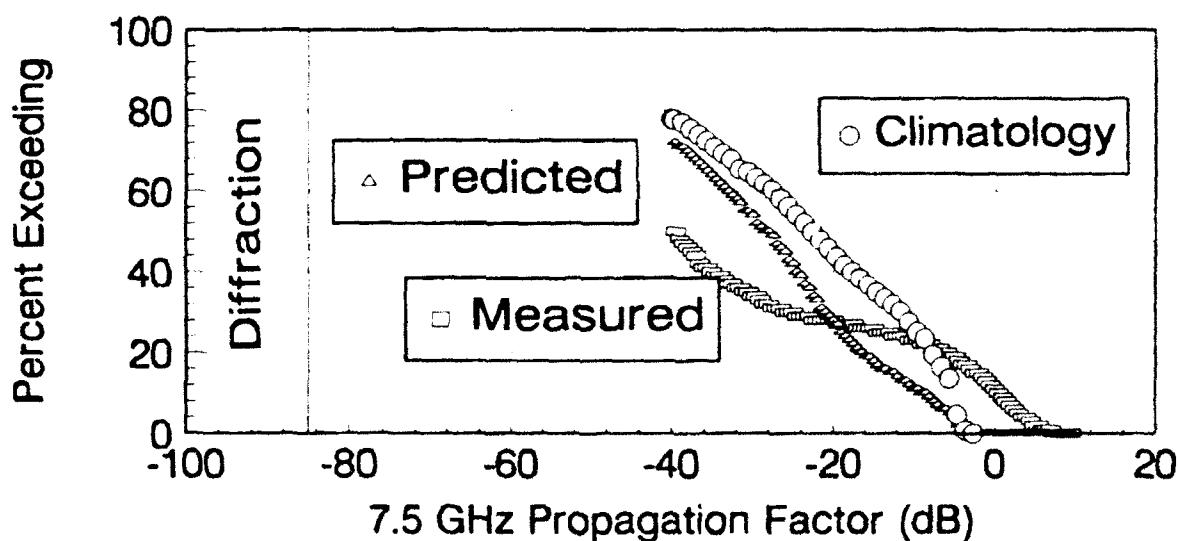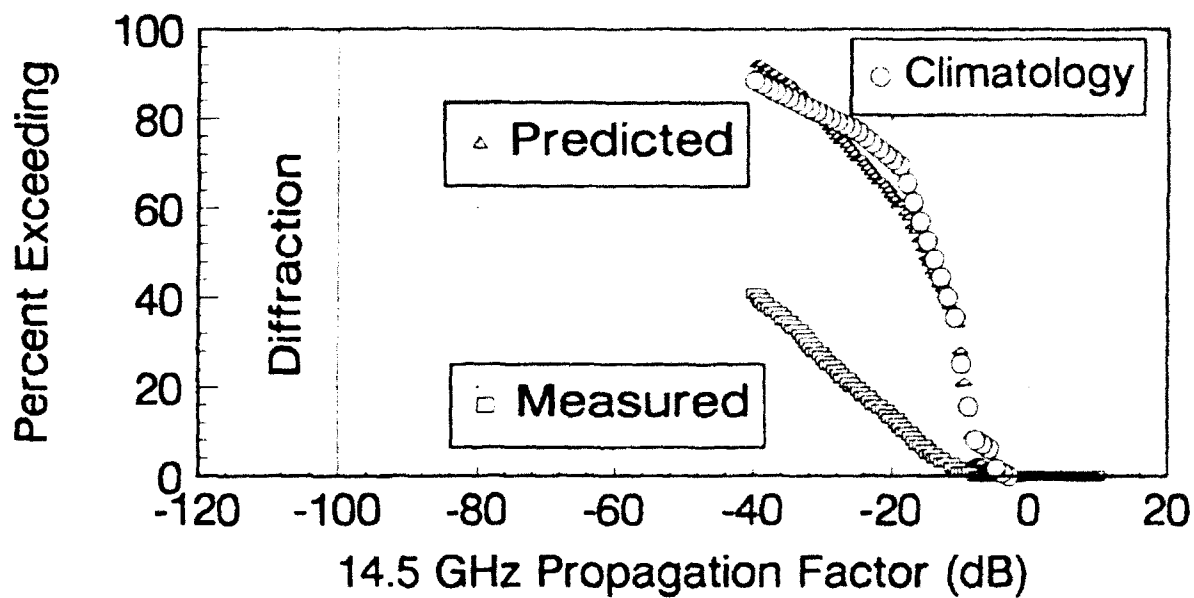
33

Figure 23. Cumulative distributions of climatology predicted, meteorological measurement predicted, and measured propagation factors.

At 7.5 GHz, the 50% point on the ordinant of the *Measured* curve is offset 16 dB to the left of the *Climatology* curve and 12 dB to the left of the *Predicted* curve. Likewise, the propagation factor corresponding to 10^{-6} BER is −30 dB; *Climatology*, *Predicted*, and *Measured* propagation factors exceed this value 54, 62, and 34% of time, respectively.

Cumulative distributions of percent error-free seconds, figure 24, correspond with those of the propagation factors. For a time-varying signal, it is expected that when the average propagation factor over some moderate time interval is equal to the propagation factor corresponding to error-free communications (10^{-6} BER), the percentage of time when the signal is error free will be 50%. As stated before, at 14.5 GHz, the availability of the signal

above the error-free threshold is 27%. From figure 24 it is seen that 26% of the time the percent error-free seconds exceeds 50%. At 7.5 GHz, the availability of the signal above the error-free threshold is 34%, and 32% of the time, the percent error-free seconds exceeds 50%.
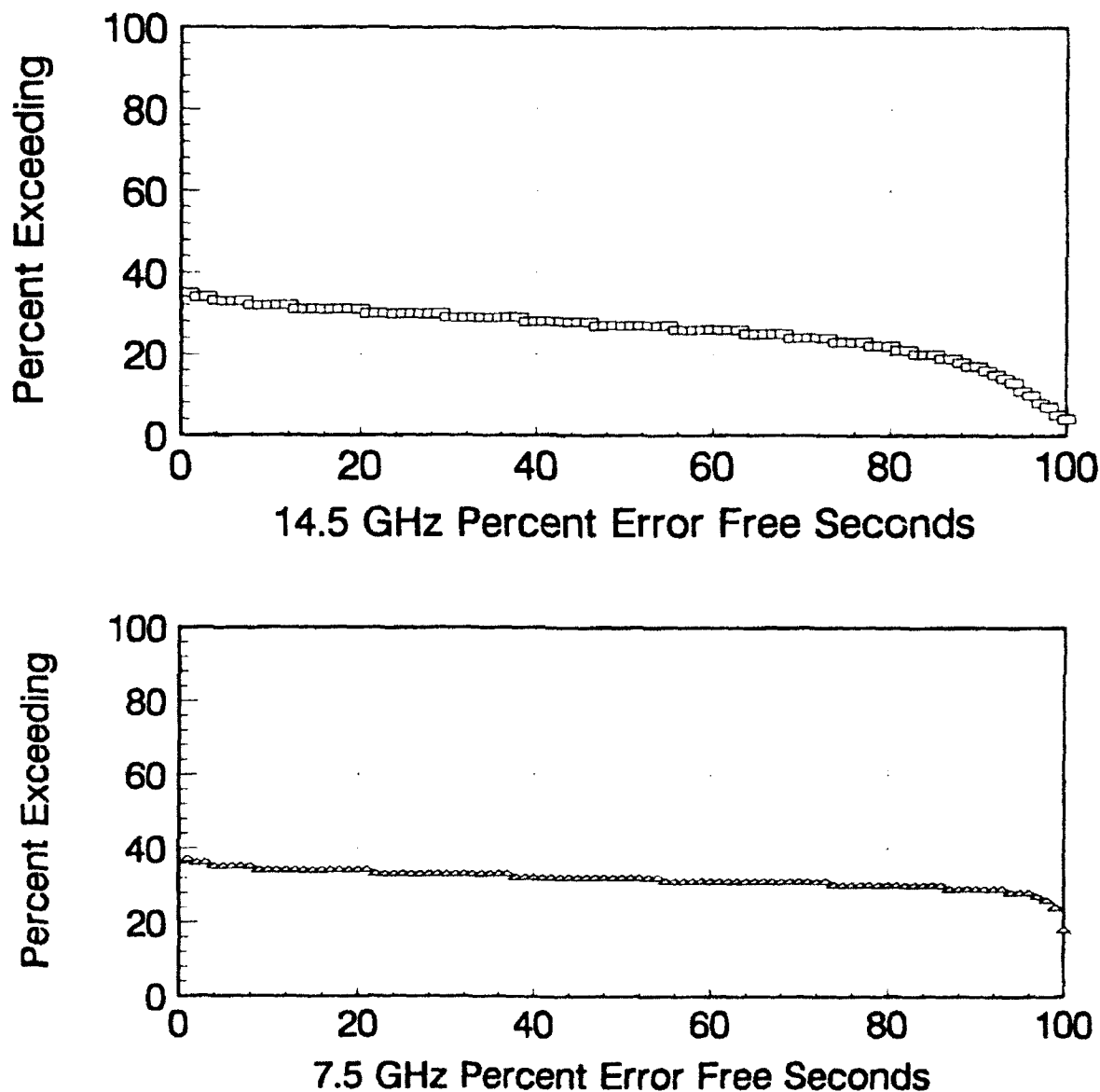

Figure 24. Cumulative distribution of percent error-free seconds (%EFS).

Consideration of the geographical aspects of EDCOM suggests differentiating between *Onshore* flow as opposed to *All Cases* that have been discussed so far. Meteorological instruments for EDCOM are located at the transmit and receive site on the shoreline. With onshore flow (sea breeze), the air mass has traveled over the water and its bulk parameters (air temperature, wind speed, and relative humidity) should be representative of the air mass over the propagation path. During *Offshore* flow, the air mass has not traveled over the body of water and its bulk parameters may not be representative of those over the

propagation path. Figure 25 shows *Measured* and *Predicted* propagation factor distributions at 14.5 and 7.5 GHz during periods of onshore flow. The difference between the distributions of *Measured* and *Predicted* propagation factors during periods of *Onshore* flow does not differ appreciably from the differences between the distributions of *Measured* and *Predicted* propagation factor for *All Cases*. At 14.5 GHz and during *Onshore* flow, the 36% point on the ordinant of the *Measured* curve is offset 29 dB to the left of the *Predicted* curve. At 7.5 GHz, the *Measured* curve at the 47% point is offset 15 dB to the left of the *Predicted* curve. This is a 2 to 3 dB greater difference than seen when considering all cases.
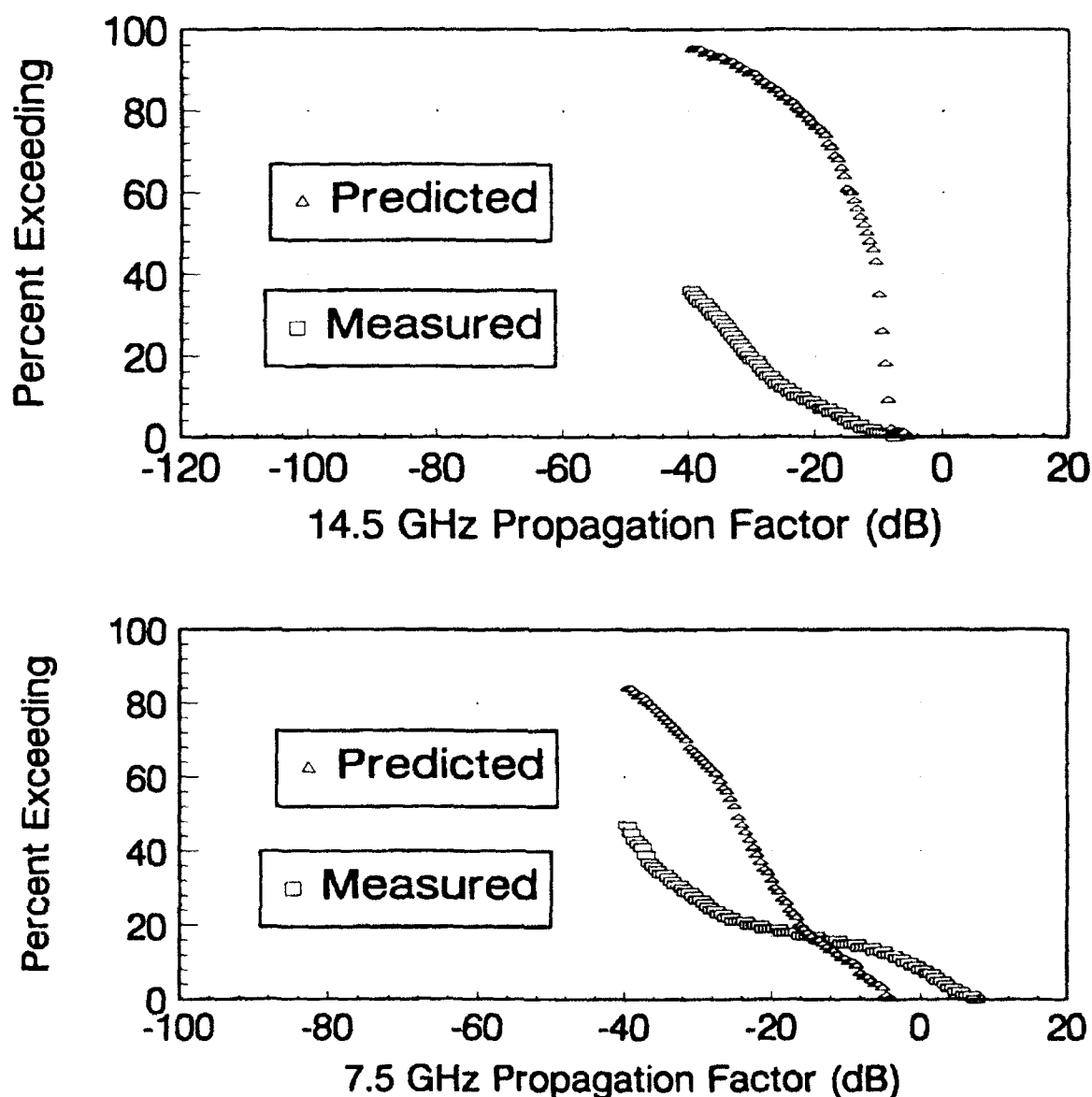

Figure 25. Cumulative distribution for meteorological measurement predicted and measured propagation factor for onshore flow.

A major goal of EDCOM is evaluating the performance of *MLAYER* in predicting propagation factors for a given evaporation duct height. Figure 26 is a scatter plot of observed propagation factors versus evaporation duct height. *MLAYER* predicted propagation factors for a neutral atmosphere are plotted as a solid line. On the 7.5-GHz plot, there is a well-defined clustering. The upper cluster (average propagation factor equal to zero) is most likely due to the effects of surface-based ducts from elevated trapping layers (not evaporative ducting). At evaporation duct heights greater than 15 m, the distribution does not appear bi-modal. The 14.5-GHz plot does not show the clustering seen at 7.5 GHz when the evaporation duct height is less than 15 m.
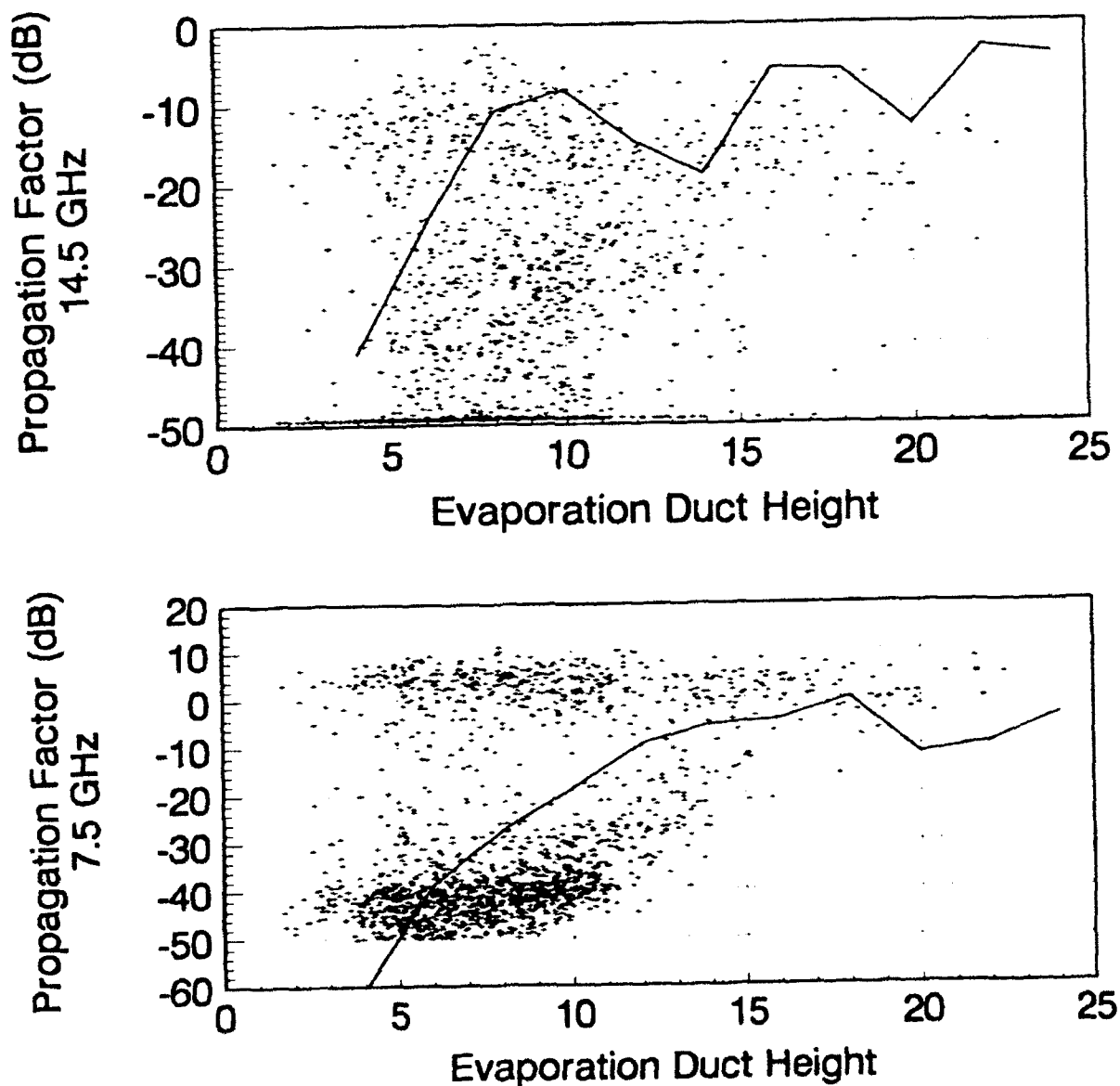

Figure 26. Propagation factor versus evaporation duct height for hour averaged propagation factors. The solid lines are model predictions based upon neutral evaporation duct profiles.

To assess the feasibility of using the evaporation duct as an alternative communications channel, it is necessary to separate those observations where the evaporation duct is not the dominant mode of propagation, from those where it is. Figure 27 plots hour averages of measured propagation factors that are within 2 hours of an atmospheric refractivity profile labeled STD or SBD in figure 8 or 9. The crosses indicate that the measurement is associated with a standard or nearly standard (STD) refractivity profile, and the triangles are associated with surface-based ducts (SBD). At 7.5 GHz, roughly half of the measurements associated with surface-based duct profiles (triangles) are clustered with propagation factors ranging from −10 dB to +5 dB, seemingly independent of the evaporation duct height. The appearance of the surface-based duct associated measurements at 14.5 GHz is similar, except for the upper clustering of propagation factors for the surface-based ducts ranging from −20 to −10 dB. The remainder of the SBD hour averages at both frequencies are evenly distributed with the STD hour averages.

Measurements where the evaporation duct is the dominant mode (crosses) tend to follow the *MLAYER* prediction curve clearly at 7.5 GHz and less clearly at 14.5 GHz. It is observed that almost all of the STD measurements at 7.5 GHz are in the lower cluster of measurements. Receiver performance, however, must be taken into account when comparing propagation factors for a given evaporation duct height for the cases where the evaporation duct is the dominant mode of propagation. From figure 7, it is seen that the AGC voltage no longer varies linearly with received signal level when the propagation factor is less than −50 dB at either frequency. This implies that −50 dB is the lowest measured propagation factor that may be used confidently for analysis. When the evaporation duct height drops below 9 m, at either frequency, many measurements in the lower or evaporative ducting cluster are less than −50 dB. There are also very few observations at duct heights greater than 17 m.

Figure 28 is similar to figure 27, except that only STD observations are plotted, and two linear least squares fit lines have been included on each graph for observations where the evaporation duct height is greater than 9 m and less than 17 m. In both figures, the upper least squares line is from all evaporative ducting observations. The upper line at 7.5 GHz is approximately 10 dB less than predicted values. The upper line at 14.5 GHz is approximately 20 dB less than predicted values. It is felt that the upper cluster of measurements in the 7.5 GHz plot is due to surface-based ducts that are not reflected by associated atmospheric sounding of figures 8 and 9 due to spatial and temporal variations. The lower least squares line for both graphs is developed by considering only those observations where propagation factor is less than −10 dB at 7.5 GHz. The line at 7.5 GHz is approximately 7 dB less than predicted values, and the line at 14.5 GHz is approximately 23 dB less than predicted values. It is felt that when the evaporation duct is the dominant mode of propagation, and the evaporation duct height is between 9 and 17 m, the mean value for propagation factors will be within a few dB of the lower least squares line and will not exceed the upper least squares line.
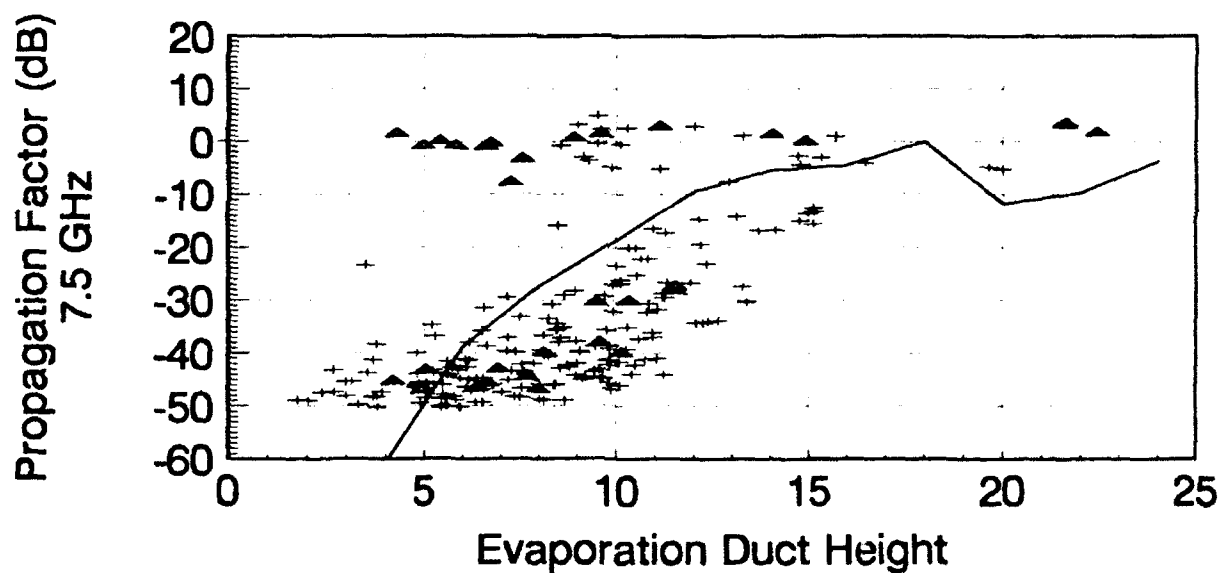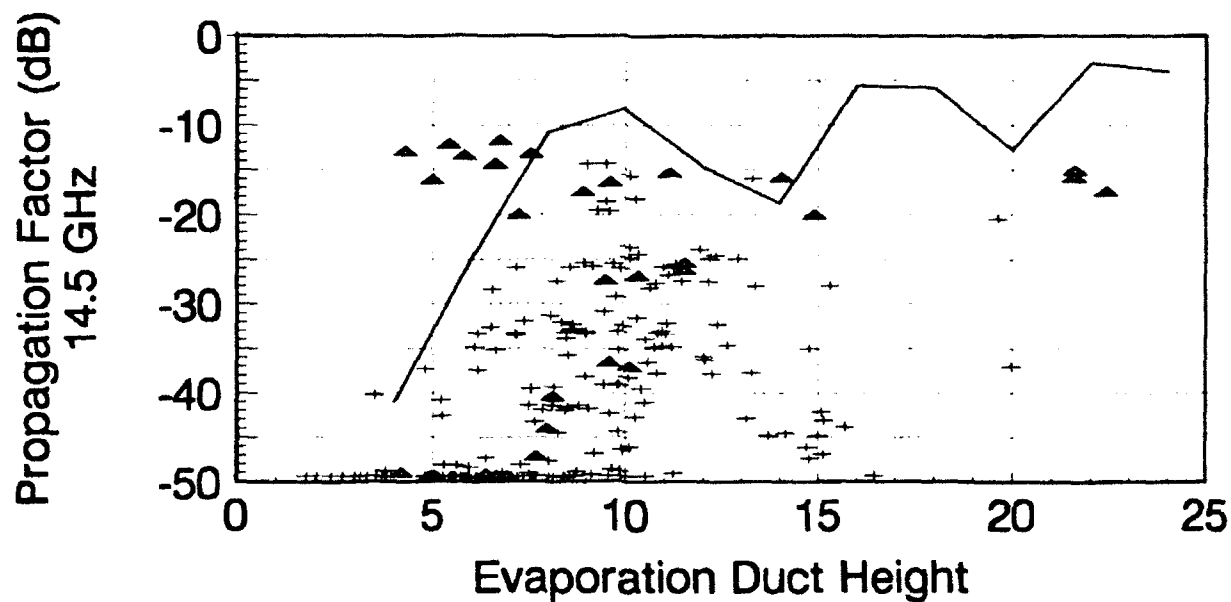
Figure 27. Propagation factor versus evaporation duct height separating surface and elevated duct observations (triangles) from purely evaporative ducting cases. The solid lines are model predictions based upon neutral evaporation duct profiles.
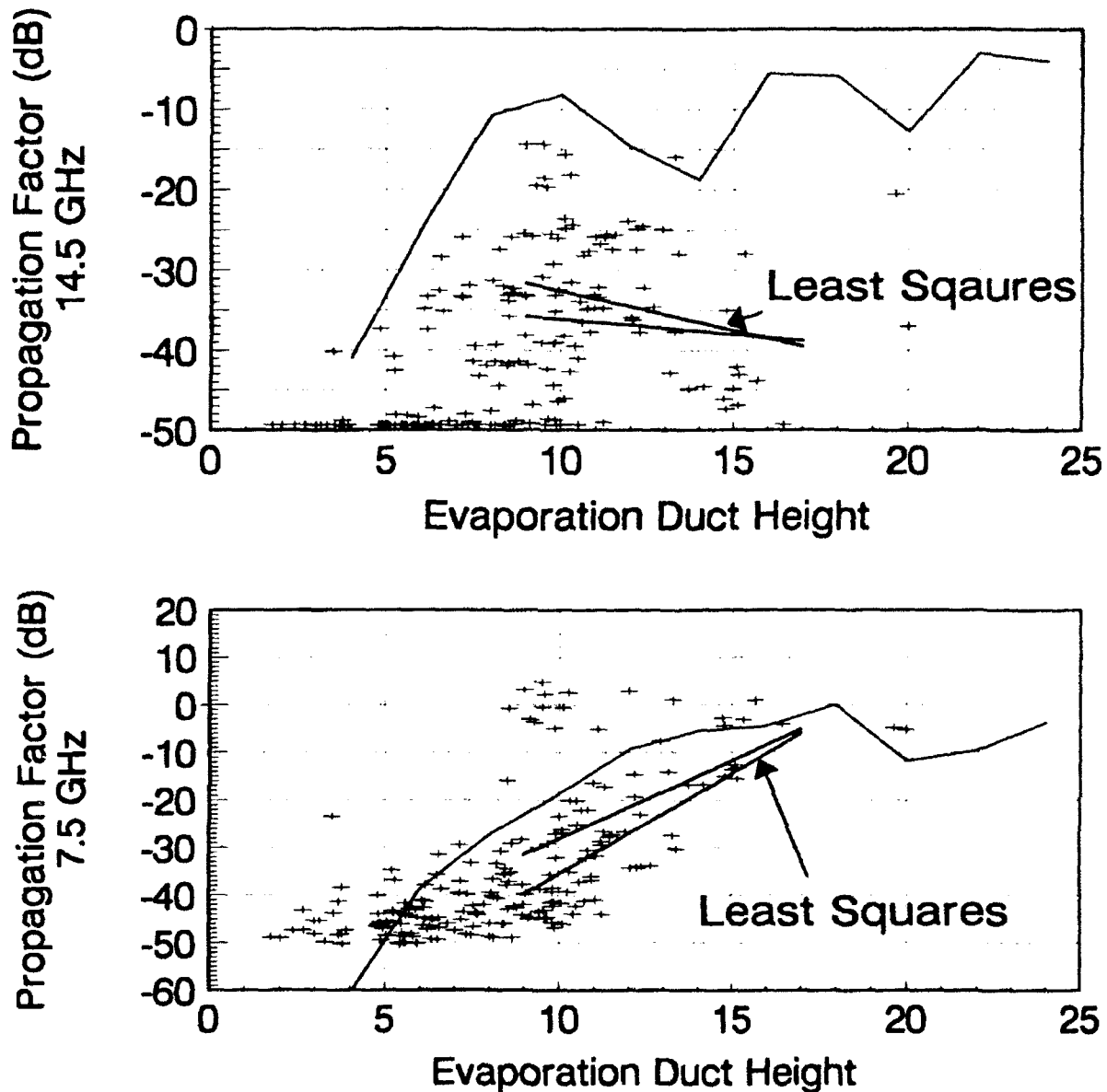
Figure 28. Propagation factor versus evaporation duct height from purely evaporative ducting cases with linear least squares fit lines for evaporation duct heights between 9 and 17 meters. Unmarked solid lines on each graph are model predictions based upon neutral evaporation duct profiles.

The differences between predicted and measured signal strength are primarily due to horizontal inhomogeneity. Those periods, where the evaporation duct is the dominant mode of propagation and the winds are light, have the lowest evaporation duct heights. Light winds are normally associated with considerable variability of both wind speed and wind direction. As a result, there are considerable differences in wind speed and direction, and therefore a difference in the evaporation duct height along the path. The nonuniformity of the duct may increase the leakage from it, and it may, consequently, reduce the

receive site signal levels. At higher wind speeds, both wind speed and direction are normally more uniform. This implies less variability along the path, and a more uniform duct that minimizes leakage. This may explain the much closer match between prediction and measurement at higher evaporation duct heights.

HIGH SPEED TESTS

For a normal (line-of-sight) microwave communications system, *multipath fading* (Livingston, 1970) is the term used to describe signal strength variation due to phase differences between reflected/refracted rays. For ducted communications, there may be no significant direct or nonreflected/refracted rays, but rather there may be many different, competing rays. Rapid local variations in the atmospheric structure along the propagation path bring changes in field strength and phase for any particular mode at the receive site. The time-dependent interference of these modes leads to large signal variations. Again, determining the micro-meteorology along the path is not practical, so fading characteristics are determined experimentally by high-speed sampling of the propagation factor.

Over 400 time series, having a one-second (1-Hz) sample interval over a 250 second duration, were taken of propagation factor and bit-error rate during the course of EDCOM. Figure 29 illustrates propagation factors from one time series taken at 1500T, 9 February 1992. From figure 8, it is seen that this is a period when the evaporation duct is the dominant mode of propagation. For both frequencies, the signal usually stays within 3 dB of the median value (propagation factors of approximately −20 dB at 7.5 GHz, and −26 dB at 14.5 GHz). This is fairly typical of the type of time series seen when evaporation ducting is dominant. Figure 30 is similar to figure 29, except that it was taken at 1500T on 24 February 1992 during surface ducting conditions. The two major differences between these periods are the higher signal levels and greater fading experienced with the surface ducting conditions. Figure 30 may be considered typical of the conditions seen during surface-based ducting conditions.

If figures 29 and 30 are truly typical of conditions where the dominant modes of propagation are the evaporation ducting and surface-based ducts, respectively, then it is to be expected that propagation factors during surface-based ducting conditions will be distributed more widely about the mean value for 5-minute samples than those taken during evaporation ducting conditions. From the discussion of long-term time series and cumulative distributions, it is seen that when the evaporation duct is the dominant mode of propagation, and when it is less than 15 m, propagation factors at 7.5 GHz are typically less than −10 dB. With very thick ducts, either surface-based ducts or duct heights greater than 15 m, the propagation factors typically exceed −10 dB. Figure 31 plots distribution (thick line) and density (thin line) of one-second samples for all time series when the mean propagation factor at 14.5 GHz is greater than −30 dB, and at 7.5 GHz, mean PF was less than −20 dB, conditions typically associated with those times where the evaporation duct is the dominant mode of propagation. Figure 32 is similar, except it has been developed from time series where the propagation factor at 7.5 GHz exceeded -10 dB. Taking numbers from the graph, it is seen that, with the evaporation duct, less than 5% of the samples are
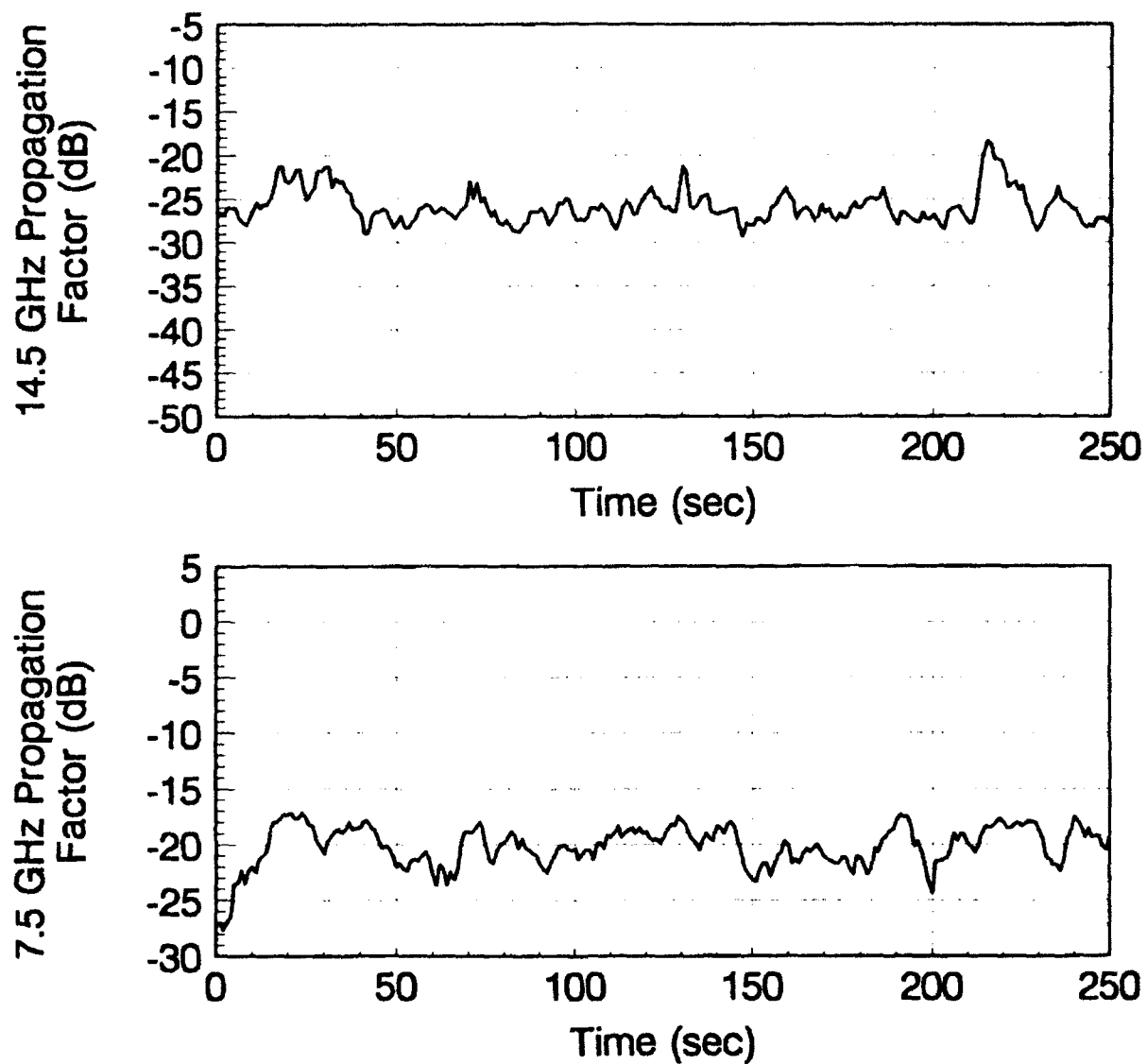
41

Figure 29. 1-Hz sampling of 250-second time series of 1500T, 9 February 1992. Evaporative ducting is dominant mode of propagation.
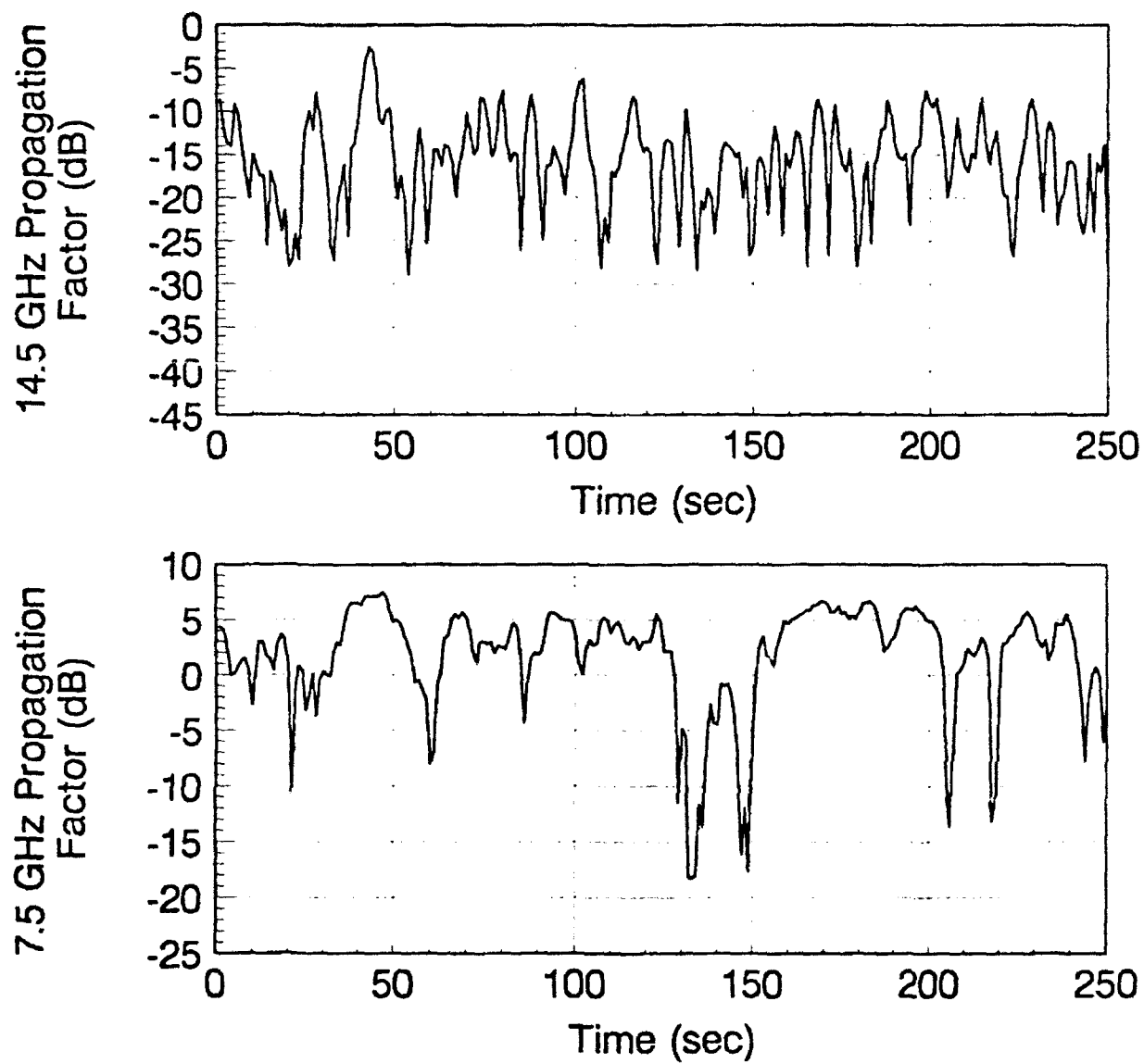
Figure 30. 1-Hz sampling of 250-second time series of 1500T, 24 February 1992. A surface based duct is the dominant mode of propagation.
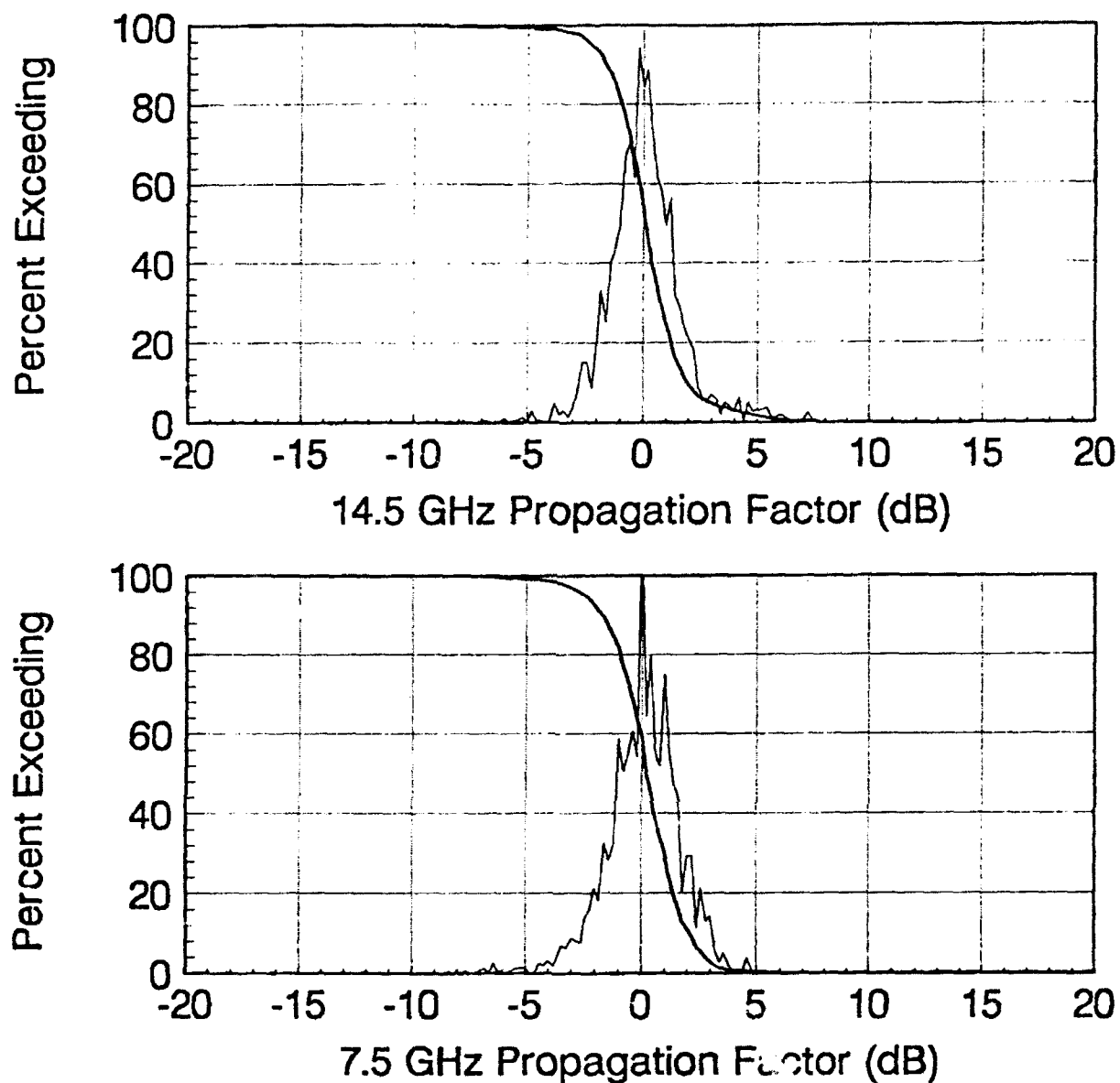
Figure 31. Distribution and density of difference between 1-Hz samples and mean value of 250-second time series of propagation factors where the evaporation duct is the dominant mode of propagation.
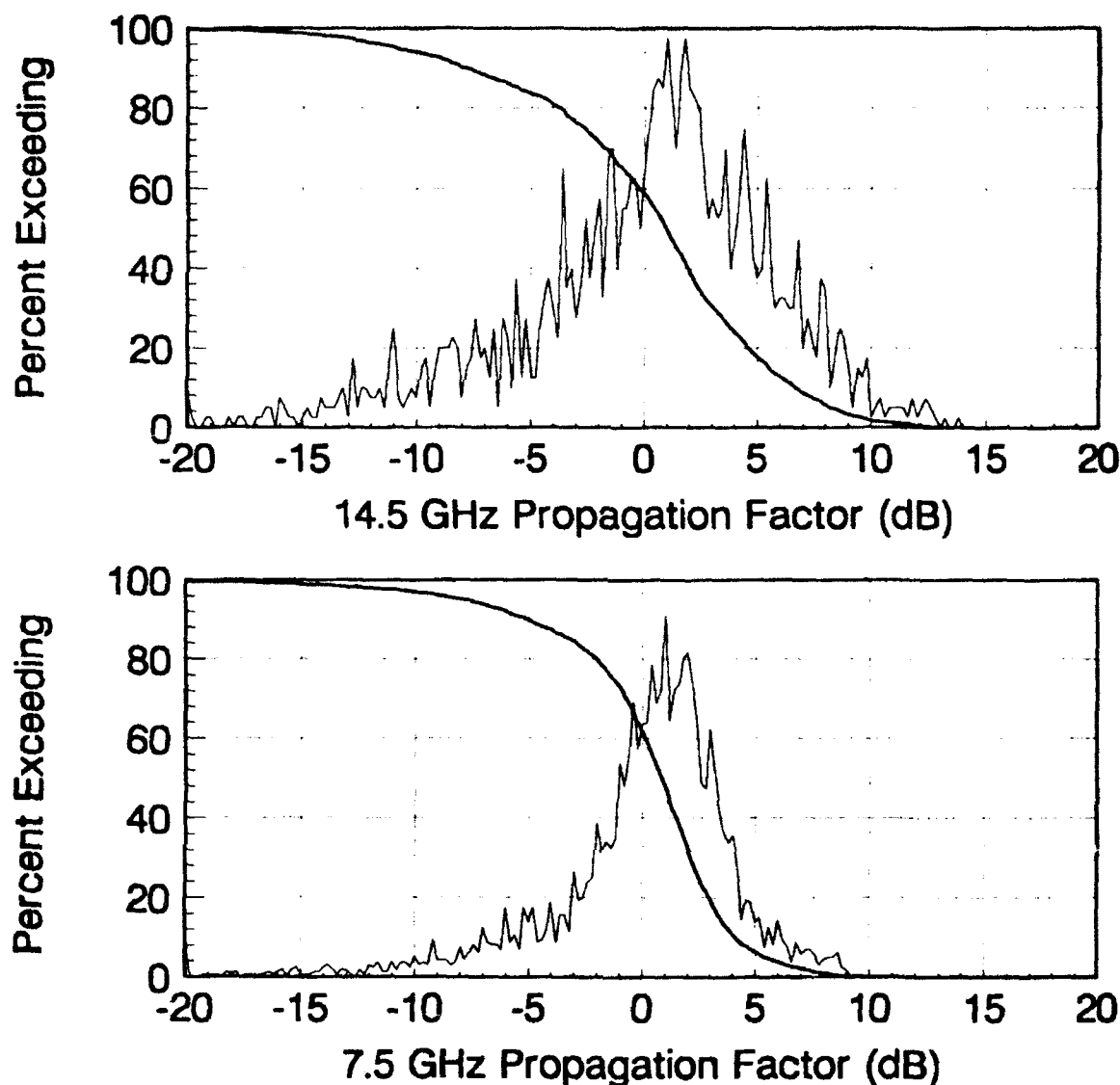
Figure 32. Distribution and density of difference between 1-Hz samples and mean value of 250-second time series of propagation factors where the evaporation duct is not the dominant mode of propagation.

3 dB or more down from the mean signal strength (at zero). Under the conditions where the evaporation duct is not the dominant mode, or the duct height is greater than 15 m, 5% of the measurements are 10 dB (or more) down from the mean signal strength.

Bit-error rates closely following the sampled propagation factor suggest that significant aliasing has not occurred in the sampling of the propagation factor. Figures 33 and 34 are 250-second time samples of both propagation factor and bit-error rate at 14.5 and 7.5 GHz, respectively; each taken at a period of time when the signal has been near the signal level where the BER is 10^{-6}. On both figures, the bit errors closely follow the sampled propagation factor. It is also seen at the 14.5-GHz time series, in figure 33, that 10^{-6} BER corresponds to a propagation factor of roughly -30 dB; and at 7.5-GHz time series, in figure 34,

that 10^{-6} BER corresponds to a propagation factor of roughly -29 dB. These values agree closely with the values plotted in figure 7 for bit-error rate versus propagation factor.
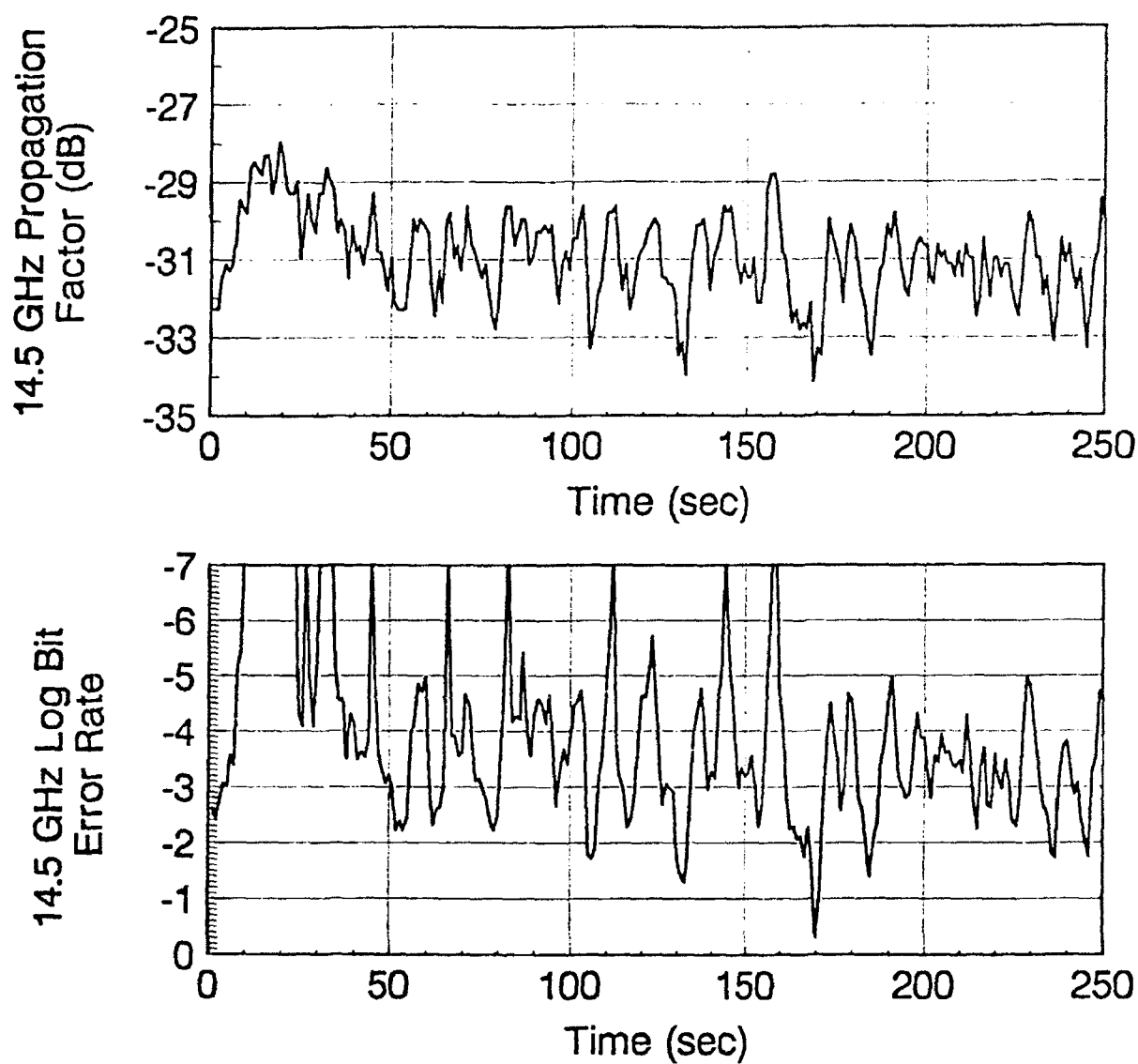

Figure 33. One-second interval sampling of propagation factor and bit-error rate of 14.5-GHz signal at 1500T on 3 March 1992.
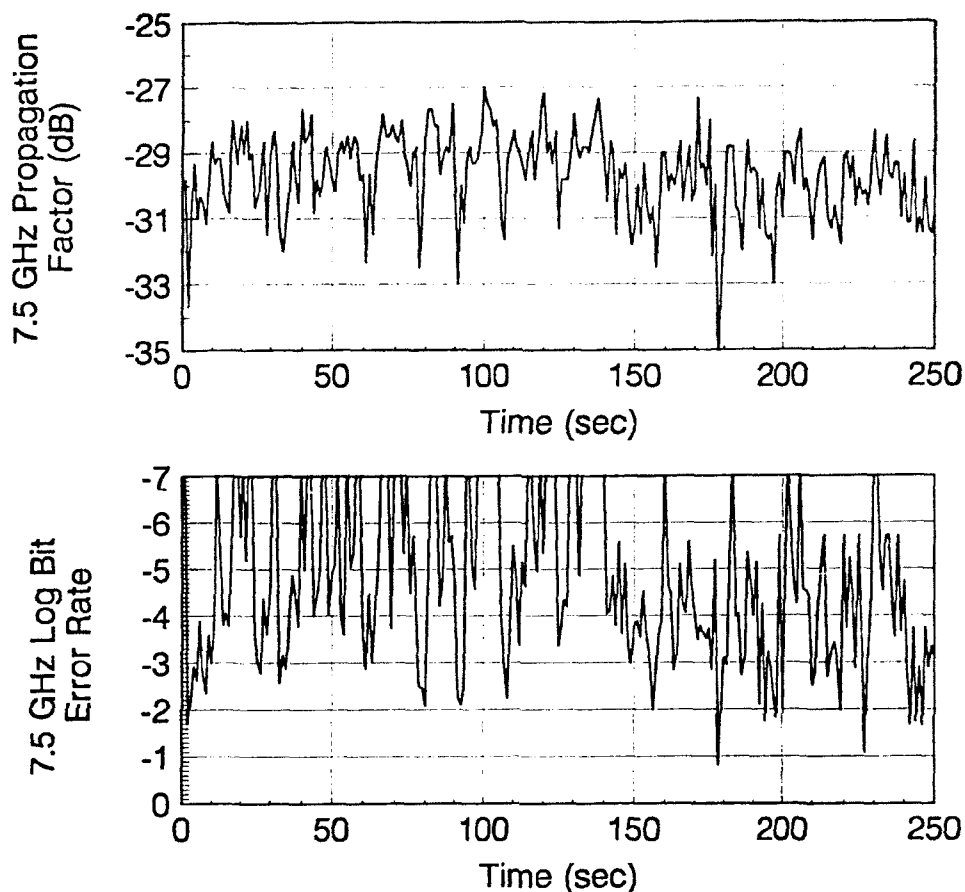
Figure 34. One-second interval sampling of propagation factor and bit-error rate of 7.5-GHz signal at 1500T on 17 February 1992.

To provide further information on the time-varying nature of the channel, 4096-point time series at 200 Hz-rate were taken of the propagation factor at both frequencies. On 21 July 1992, propagation factors at both frequencies were in the linear range of the receiver, and average signal levels indicated the evaporation duct was the dominant mode of propagation. Figure 35 shows the first of the described time series taken on that date. At both frequencies, it is seen that clearly identifiable minimums occur at intervals ranging from 0.5- to 2-seconds. Intervals from deeper minimums occur at larger time intervals. Averaged, Parzan (triangular) windowed power spectrum were developed using nine consecutive sets of the described 4096-point time series. The results are displayed in figure 36. It is observed that contribution of frequency components drops rapidly and that the spectrum is

47

essentially flat at frequencies above 10 Hz. This finding agrees with the discussion of bit-error rates and propagation factors in the preceding paragraph.
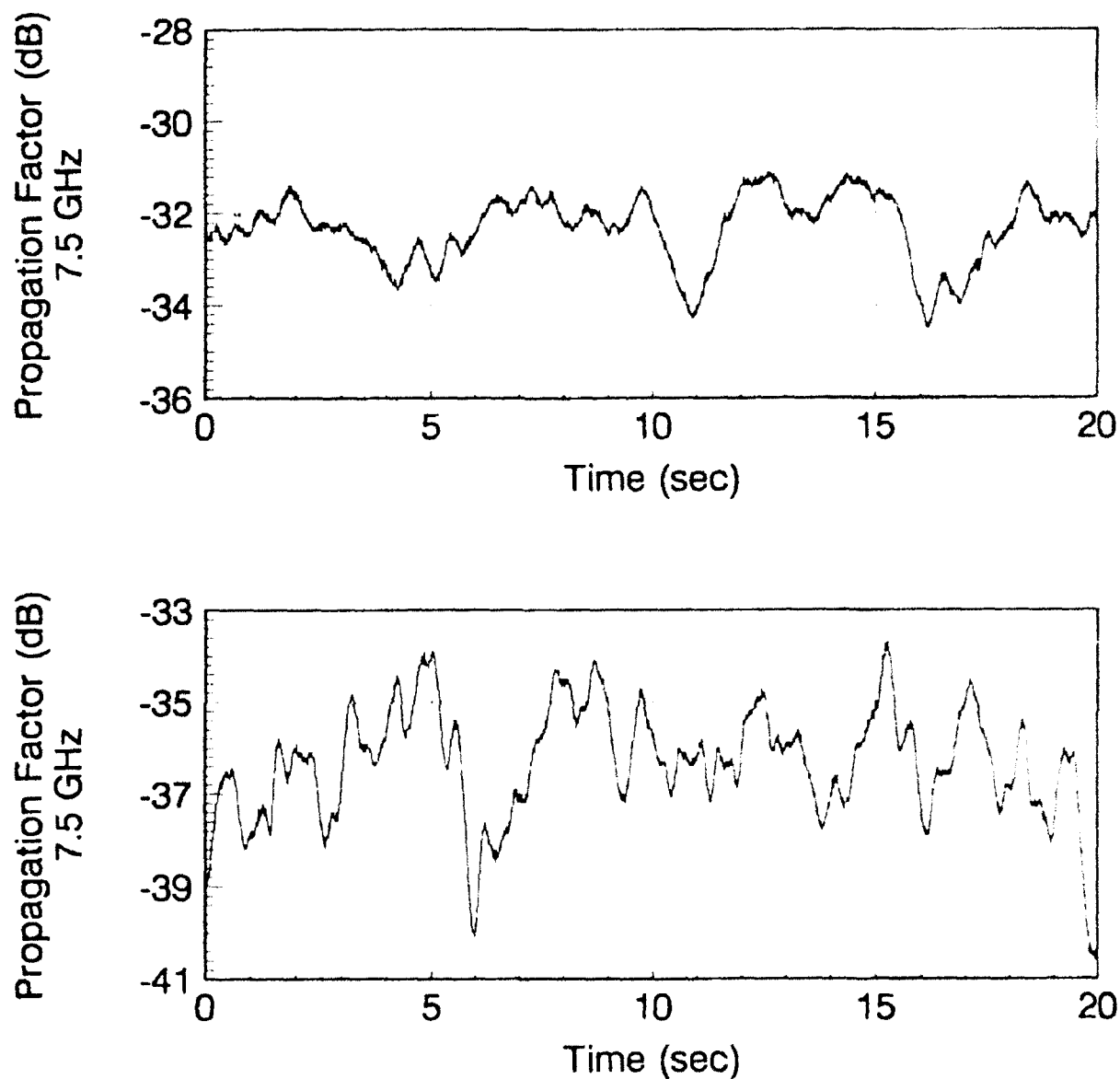
Figure 35. 20-Hz sample rate time series of propagation factors taken 21 July 1992.
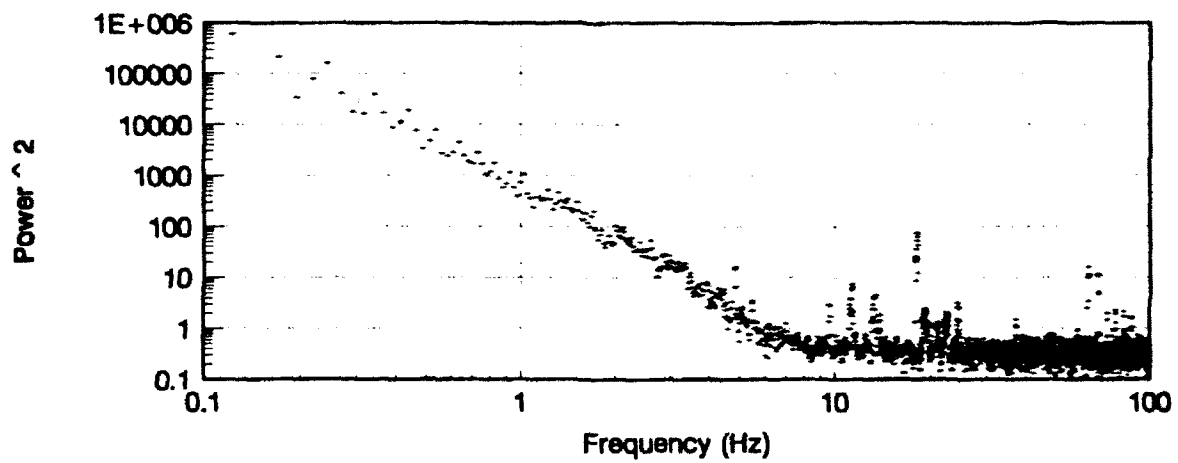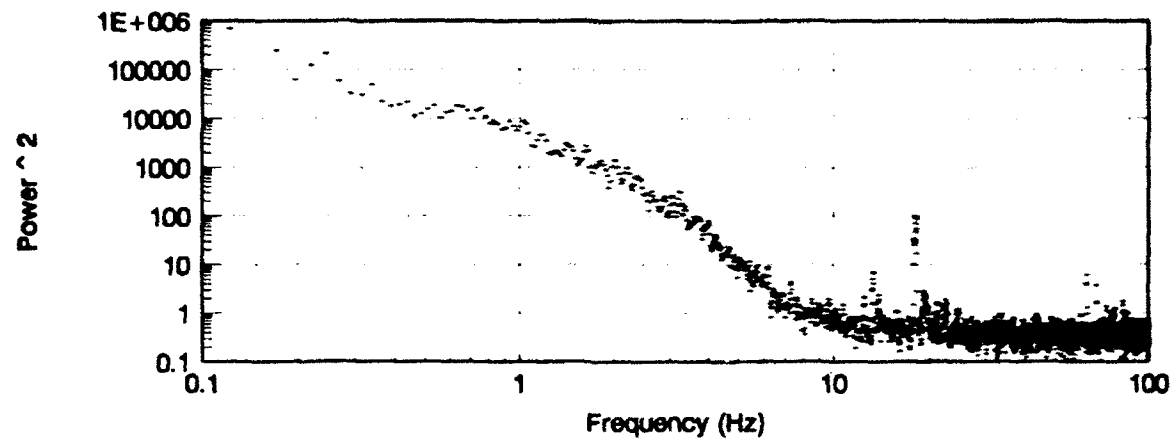
Figure 36. Power spectrum from series of nine, 4096-point, 20-Hz sample rate time series of 21 July 1992.
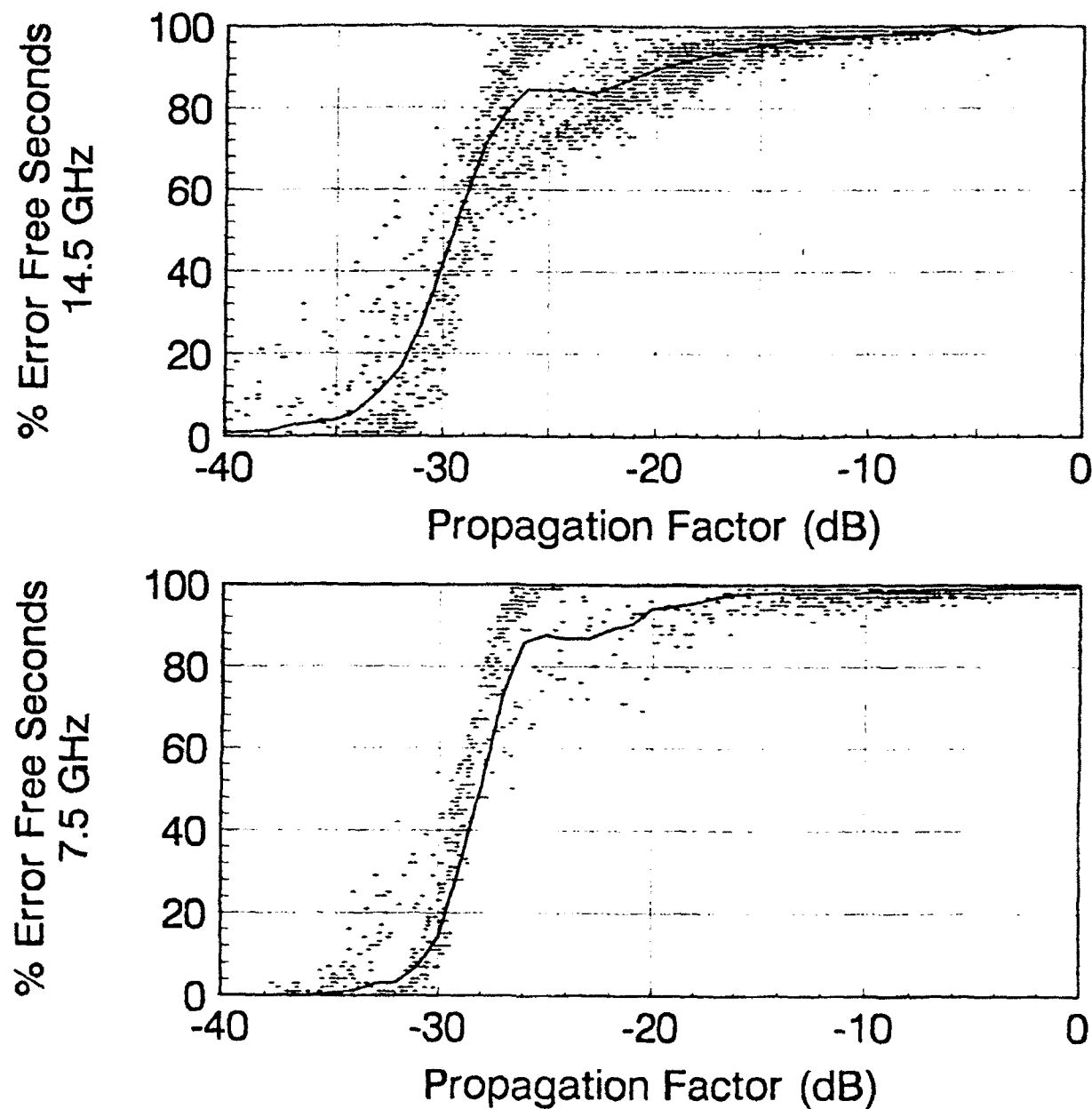
Figure 37. Scatter plot of percent error-free seconds (%EFS) versus propagation factor.

DIGITAL SYSTEM PERFORMANCE

The quality of the channel for digital communications is significantly affected by signal fluctuations. It is desired to determine how much power beyond the steady power required for 10^{-6} BER is required to ensure the %EFS exceeds a given value. Figure 37 provides scatter plots and mean values for %EFS as a function of ARSL at both frequencies. At 7.5 GHz, -28 dB corresponds to a 50 %EFS. From figure 7, it is seen that 10^{-6} BER corresponds to approximately -30 dB propagation factor. At 14.5 GHz, there is a similar

correspondence. Using round figures at both frequencies, 4 dB of additional power will provide 80% error-free seconds; 10 dB extra will provide 90% error-free seconds.

CONCLUSIONS

The evaporation duct strongly influences low-altitude, over water, over-the-horizon propagation at microwave frequencies. For the geometry and conditions of the EDCOM experiment, the evaporation duct substantially enhances signal strengths above the diffraction field levels. At 14.5 GHz, the average enhancement is roughly 50 dB; at 7.5 GHz the average enhancement is typically 40 dB. At 14.5 GHz the degree of enhancement is typically 20 to 30 dB less than model prediction. At 7.5 GHz the enhancement is typically 15 dB less than prediction with the difference between modeled and measured values decreasing with increasing evaporation duct height.

Digital signal quality is affected by variations in signal strength. Fading of the signal requires an increase of power above that level associated with error-free communications for a constant signal level, to achieve a desired percentage of time when the channel is error free. At both frequencies, 4 dB of additional power will provide 80% error-free seconds; 10 dB extra will provide 90% error-free seconds. Obviously these figures apply only to the path and conditions of EDCOM. During conditions where the evaporation duct is the dominant mode of propagation, most fading events are within 5 dB of the 5-minute average signal level. Fading events during surface-based ducting are much deeper than those during evaporation ducting, often 20 dB or more. Note, however, that with surface-based ducting, signal levels approach free space at 14.5 GHz and often exceed free space levels at 7.5 GHz.

51

REFERENCES

Anderson, K. D. 1991. "Evaporation Duct Communication: Test Plan," NRaD TD 2033 (Feb.). Naval Ocean Systems Center, San Diego, California.

Anderson, K. D. 1990. "94-GHz Propagation in the Evaporation Duct," IEEE Trans. Ant. and Prop., vol. 38, no. 5.

Baumgartner, G. B., Jr. 1983. "XWVG: A Waveguide Program for Trilinear Tropospheric Ducts," NOSC TD 610 (June). Naval Ocean Systems Center, San Diego, California.

Budden, K. G. 1961. *The Waveguide Mode Theory of Wave Propagation*. Logos, London, England.

Hitney, H.V., J. H. Richter, R. A. Pappert, K. D. Anderson, and G. B. Baumgartner, Jr. 1985. "Tropospheric Radio Wave Propagation," Proc. IEEE, vol. 73, no. 2.

Hitney, H. V. 1975. "Propagation Modeling in the Evaporation Duct," Naval Electronics Lab. Cen. Tech. Rep. 1947 (April). Naval Ocean Systems Center, San Diego, California.

Jeske, H. 1971. "The State of Radar-Range Prediction Over Sea," Tropospheric Radio Wave Propagation Part II, AGARD, pp. 50-1, 50-6.

Katzin, M., R.W. Bauchman, and W. Binnian. 1947. "3- and 9-Centimeter Propagation in Low Ocean Ducts," Proc. IRE, vol. 35, no. 9, pp. 891–905.

Patterson, W. L. 1987. "Historic Electromagnetic Propagation Condition Database Description," NOSC TD 1149 (Sept.) Naval Ocean Systems Center, San Diego, California.

Paulus, R. A. 1985. "Practical Application of an Evaporation Duct Model," Radio Sci., vol. 20, pp. 887–896.

Richter, J. H., and H. V. Hitney 1988. "Antenna Heights for the Optimum Utilization of the Oceanic Evaporation Duct," NOSC TD 1209 (Jan.). Naval Ocean Systems Center, San Diego, California.

52

REPORT DOCUMENTATION PAGE

1. AGENCY USE ONLY *(Leave blank)*	2. REPORT DATE January 1993	3. REPORT TYPE AND DATES COVERED Final

4. TITLE AND SUBTITLE EVAPORATION DUCT COMMUNICATION: Measurement Results	5. FUNDING NUMBERS AC: DN300067 PE: 0602232N PN: RC32W11
6. AUTHOR(S) L. T. Rogers and K. D. Anderson	

7. PERFORMING ORGANIZATION NAME(S) AND ADDRESS(ES) Naval Command, Control and Ocean Surveillance Center (NCCOSC) RDT&E Division San Diego, CA 92152-5001	8. PERFORMING ORGANIZATION REPORT NUMBER TR 1571

9. SPONSORING/MONITORING AGENCY NAME(S) AND ADDRESS(ES) Office of Chief of Naval Research Code 396600 Arlington, VA 22217	10. SPONSORING/MONITORING AGENCY REPORT NUMBER

11. SUPPLEMENTARY NOTES

12a. DISTRIBUTION/AVAILABILITY STATEMENT Approved for public release; distribution is unlimited.	12b. DISTRIBUTION CODE

13. ABSTRACT *(Maximum 200 words)*

Results from an experiment to evaluate the performance of an overwater, over-the-horizon, SHF digital communication system are presented. Two simplex microwave digital communication circuits (similar to commercial line-of-sight microwave links) are used on an 83-km transmission path that is twice the line-of-sight distance. One circuit is operating at 7.5 GHz. The other circuit operates at 14.5 GHz. Both transmitters output a quasi-random bit stream at 1.544-megabits-per-second (DS-1) that is analyzed at the receiver site.

In a standard atmosphere, the expected received signal level (RSL) is approximately 60 dB below the receiver threshold. However, at these frequencies, propagation modeling shows that, more than half of the time, trapping by the evaporation duct can increase RSL by at least 60 dB.

The propagation path is instrumented at both ends to record surface meteorological conditions and RF characteristics. RSL measurements are compared to predicted levels which are derived from the measured surface meteorology. Industry standard digital performance measurements are used to assess the effect of RSL variation on link performance. Additionally, results from high-speed sampling of RSL are made to assist in channel characterization.

14. SUBJECT TERMS Super High Frequency Radio communications SHF			15. NUMBER OF PAGES 63
			16. PRICE CODE

17. SECURITY CLASSIFICATION OF REPORT UNCLASSIFIED	18. SECURITY CLASSIFICATION OF THIS PAGE UNCLASSIFIED	19. SECURITY CLASSIFICATION OF ABSTRACT UNCLASSIFIED	20. LIMITATION OF ABSTRACT SAME AS REPORT

21a. NAME OF RESPONSIBLE INDIVIDUAL	21b. TELEPHONE *(Include Area Code)*	21c. OFFICE SYMBOL
L. T. Rogers and K. D. Anderson	(619) 553–1413	Code 543

INITIAL DISTRIBUTION